MIT Libraries | DSpace@MIT

MIT Open Access Articles

Covariation of climate and long-term erosion rates across a steep rainfall gradient on the Hawaiian island of Kaua'i

The MIT Faculty has made this article openly available. ***Please share*** how this access benefits you. Your story matters.

Citation: Ferrier, K. L., J. T. Perron, S. Mukhopadhyay, M. Rosener, J. D. Stock, K. L. Huppert, and M. Slosberg. "Covariation of Climate and Long-Term Erosion Rates Across a Steep Rainfall Gradient on the Hawaiian Island of Kaua'i." Geological Society of America Bulletin 125, no. 7–8 (July 1, 2013): 1146–1163.

As Published: http://dx.doi.org/10.1130/B30726.1

Publisher: Geological Society of America

Persistent URL: http://hdl.handle.net/1721.1/85607

Version: Author's final manuscript: final author's manuscript post peer review, without publisher's formatting or copy editing

Terms of use: Creative Commons Attribution-Noncommercial-Share Alike

Massachusetts Institute of Technology

Covariation of climate and long-term erosion rates across a steep rainfall gradient on the Hawaiian island of Kaua‘i

Ken L. Ferrier[1], J. Taylor Perron[1], Sujoy Mukhopadhyay[2], Matt Rosener[3], Jonathan D. Stock[4], Kimberly L. Huppert[1], Michelle Slosberg[1]

[1] *Department of Earth, Atmospheric, and Planetary Sciences, Massachusetts Institute of Technology, Cambridge, MA*

[2] *Department of Earth and Planetary Sciences, Harvard University, Cambridge, MA*

[3] *U.S. Geological Survey, Hanalei, Kaua‘i, HI*

[4] *U.S. Geological Survey, Menlo Park, CA*

ABSTRACT

Erosion of volcanic ocean islands creates dramatic landscapes, modulates Earth's carbon cycle, and delivers sediment to coasts and reefs. Because many volcanic islands have large climate gradients and minimal variations in lithology and tectonic history, they are excellent natural laboratories for studying climatic effects on the evolution of topography. Despite concerns that modern sediment fluxes to island coasts may exceed long-term fluxes, little is known about how erosion rates and processes vary across island interiors, how erosion rates are influenced by the strong climate gradients on many islands, and how modern island erosion rates compare to long-term rates. Here we present new measurements of erosion rates over 5-year to 5-million-year timescales on the Hawaiian island of Kaua‘i, across which mean annual precipitation ranges from 0.5 to

9.5 m/yr. Eroded rock volumes from basins across Kaua‘i indicate that Myr-scale erosion rates are correlated with modern mean annual precipitation and range from 8 to 335 t km^{-2} yr^{-1}. In Kaua‘i’s Hanalei River basin, ^{3}He concentrations in detrital olivines imply millennial-scale erosion rates of >126 to >390 t km^{-2} yr^{-1} from olivine-bearing hillslopes, while fluvial suspended sediment fluxes measured from 2004 to 2009 plus estimates of chemical and bedload fluxes imply basin-averaged erosion rates of 545 ± 128 t km^{-2} yr^{-1}. Mapping of landslide scars in satellite imagery of the Hanalei basin from 2004 and 2010 imply landslide-driven erosion rates of 30-47 t km^{-2} yr^{-1}. These measurements imply that modern erosion rates in the Hanalei basin are no more than 2.3 ± 0.6 times faster than millennial-scale erosion rates, and, to the extent that modern precipitation patterns resemble long-term patterns, they are consistent with a link between precipitation rates and long-term erosion rates.

INTRODUCTION

A glance at a topographic map of the Hawaiian Islands makes it clear that a great deal of rock is eroded from volcanic islands over time (e.g., Dana, 1890). The recently erupted lava flows on Mauna Loa and Kilauea volcanoes on the Island of Hawai‘i form smooth hillslopes that are undissected by rivers, and they stand in stark contrast to older Hawaiian islands like Kaua‘i, which over the past >4 Myr has been dissected by canyons more than 1 km deep. The dramatic erosion of island interiors and the correspondingly large sediment fluxes to coasts are not unique to the Hawaiian Islands, but instead are common features of many ocean islands, such as the Society Islands (e.g., Hildenbrand et

al., 2008), the Lesser Antilles (e.g., Rad et al., 2007), and Iceland (e.g., Louvat et al., 2008).

The erosion of volcanic islands offers an opportunity to investigate a number of problems central to landscape evolution. For instance, islands are isolated from continents and thus offer opportunities to investigate the co-evolution of topography and biota (e.g., Craig, 2003). Because islands are small, they offer an opportunity to study how boundary effects propagate through landscapes. Volcanic islands are also well suited for isolating climatic effects on erosion, because many islands exhibit large spatial variations in climate but relatively small variations in non-climatic factors that might also affect erosion rates, such as lithology and tectonic deformation. This is particularly valuable because the effects of climate on erosion rates are a matter of long-standing and continuing debate (e.g., Langbein and Schumm, 1958; Riebe et al., 2001; DiBiase and Whipple, 2011), and because attempts to measure climatic effects on erosion rates are often confounded by site-to-site variations in non-climatic factors (e.g., Walling and Webb, 1983; von Blanckenburg, 2005). Furthermore, climate's effect on erosion rates is often cited as the driver for an important feedback in the co-evolution of climate, topography, and mountain structure (e.g., Willett, 1999; Beaumont et al., 2001; Whipple and Meade, 2004; Stolar et al., 2007; Roe et al., 2008; Whipple, 2009), and despite a few observations of correlations between precipitation rates and erosion rates (e.g., Reiners et al., 2003; Owen et al., 2010; Moon et al., 2011), there remains no empirical consensus on the net effects of climate on erosion rates. Lastly, volcanic islands are examples of transient landscapes, with topography that is lowered by both surface erosion and island subsidence. This distinguishes islands from many continental settings in which rock

uplift counterbalances erosion, driving the topography toward an approximate steady state (e.g., Hack, 1960). Such transiently evolving landscapes are valuable because their morphologies can be more sensitive indicators of erosional processes than steady-state landscapes, which makes transient landscapes better suited for evaluating proposed models of landscape evolution (e.g., Tucker and Whipple, 2002; Tucker, 2009). Furthermore, climatic effects on erosion rates should be more apparent in transient landscapes than in steady-state landscapes, because erosion rates are governed by rock uplift rates in steady-state landscapes.

Volcanic islands thus have the potential to reveal much about landscape dynamics, and therefore have implications for continental topography as well as island topography, because erosional processes in many continental regions are similar to those on volcanic islands (e.g., Lohse and Dietrich, 2005; Jefferson et al., 2010). Yet, despite widespread attention to sediment fluxes along island coasts, comparatively little is known about how the interiors of ocean islands erode and how the dominant erosional processes and rates vary in space and time. For instance, in a study of Kaua‘i’s Waimea basin, Gayer et al. (2008) measured a 10-fold variation in cosmogenic ^{3}He concentrations among 26 samples of detrital olivine collected from a single site near the basin outlet. They suggested that this variation was best explained by spatially variable erosion rates driven by a nonlinear dependence of erosion rates on hillslope gradient. Without systematic measurements of erosional processes and rates in island interiors, it will be difficult to take full advantage of these natural experiments in landscape evolution.

The importance of such studies is augmented by societal concerns over sediment fluxes to coral reefs, where excessive sediment supply can smother reefs, reduce coral

calcification and tissue growth, inhibit larval recruitment, and restrict light from photosynthetic algae (e.g., Rogers, 1979; 1990; Cox and Ward, 2002; Telesnicki and Goldberg, 1995; Yentsch et al., 2002, Fabricius, 2005). This is a growing concern because coral reefs around the world are in rapid decline: recent surveys report that nearly 60% of global reefs may disappear by 2030 (Wilkinson, 2002; Gardner et al., 2003). To properly manage reefs, it is vital to know the long-term average rates of sediment delivery to coasts and to determine how those rates may have changed under human activity. This in turn requires erosion rate measurements over a range of timescales at a single location, ideally combined with an inventory of the erosional processes that are responsible for generating sediment.

Prior studies of steep hillslopes on the Hawaiian Islands suggest that hillslope erosion proceeds by a combination of soil creep (Wentworth, 1943; White, 1949; Scott, 1969; Scott and Street, 1976), shallow landslides in the soil (Wentworth, 1943; Ellen et al., 1993), landslides with failure in the saprolite (Peterson et al., 1993), bedrock avalanches (Jones et al., 1984), debris flows (Hill et al., 1997), and flushing of solutes (Moberly, 1963; Li, 1988). Special attention has been paid to the role of shallow landslides, since field observations of abundant landslide scars suggest that shallow landslides may be responsible for a large fraction of the mass flux from hillslopes to channels in steep Hawaiian basins (Wentworth, 1943; Scott, 1969; Ellen et al., 1993; Peterson et al., 1993). Quantifying sediment fluxes due to landslides may therefore be of central importance in sediment budgets for volcanic islands.

In this paper, we use Kaua‘i as a natural laboratory for addressing three questions central to the erosion of volcanic islands. First, how do precipitation rates affect erosion

rates on volcanic islands, and how do erosion rates vary spatially as a result? Second, how do modern erosion rates on volcanic islands compare to erosion rates over million-year and millennial timescales? Third, how important is shallow landsliding in setting erosion rates on volcanic islands? Kaua‘i is well suited for this study because it exhibits minimal variations in lithology while spanning one of Earth's steepest regional rainfall gradients, with annual rainfall rates ranging from 0.5 m/yr to 9.5 m/yr over only 25 km. To address these questions we present four new sets of erosion rate measurements on Kaua‘i, inferred from (1) the volumetric excavation of basins since the formation of the volcano surface; (2) ^{3}He concentrations in olivine grains collected in river sediment; (3) modern fluvial sediment fluxes; and (4) modern landslide inventories. We focus particular attention on Kaua‘i's Hanalei basin because previous work on sediment fluxes there provides a context for our new measurements (e.g., Calhoun and Fletcher, 1999; Draut et al., 2009; Takesue et al., 2009; Stock and Tribble, 2010), and because sediment from the Hanalei River discharges into Hanalei Bay, where high turbidity is an ecological concern (EPA, 2008; Hawaii Department of Health, 2008). In the following pages we introduce the study area on Kaua‘i, describe the methods we used to measure erosion rates, and discuss the implications of spatial and temporal variations in the measured erosion rates.

KAUA‘I GEOLOGY, TOPOGRAPHY, AND CLIMATE

Kaua‘i is the northernmost and second oldest major extant Hawaiian island. Like the other Hawaiian islands, Kaua‘i is a product of hotspot volcanism. Over 95% of Kaua'i's rock volume consists of tholeiitic basalt, which erupted during Kaua‘i's shield-

building stage 5.1-4.0 Ma and which is classified into the Na Pali Member, the Olokele Member, the Makaweli Member, and the Haupu Member (Figure 1; McDougall, 1979; Clague and Dalrymple, 1988; Garcia et al., 2010). After more than one million years of quiescence, a second stage of episodic volcanism began at ~2.6 Ma and lasted to 0.15 Ma, over which time alkalic basalts mantled about half the island (Figure 1; Garcia et al., 2010). These so-called rejuvenated lavas constitute the second major stratigraphic group on Kaua‘i, and are known collectively as the Koloa volcanics.

Unlike some younger volcanic islands, Kaua‘i has experienced major structural deformation since the growth of its initial shield, including collapse of the Olokele Caldera near the center of the island, dropdown of the Makaweli graben in the southwestern part of the island, and formation of the Lihue basin on the eastern side of the island (Macdonald et al., 1960). Some studies have suggested that Kaua‘i is not a single shield volcano but rather a composite of two shield volcanoes, on the basis of patterns in submarine rift zones and differences in Sr, Nd, and Pb isotopic compositions in basalts on the east and west sides of Kaua‘i (Clague, 1996; Holcomb et al., 1997; Mukhopadhyay et al., 2003).

Kaua‘i’s complex structural history is reflected in its topography. The eastern 10-15 km of the island is dominated by the low-lying Lihue basin, which is interpreted to have formed by structural collapse rather than by fluvial erosion (Reiners et al., 1998). By contrast, the western 5-10 km of the island is dominated by short, narrow, steep-sided canyons incised into the Na Pali Member, and is interpreted as a fluvially dissected remnant of Kaua‘i’s earliest shield surface (Figure 1). Between the eastern and western sides of the island stands the Olokele plateau, which is composed of nearly horizontal

caldera-filling lavas, and which has been incised with several canyons over 1 km deep (Macdonald et al., 1960).

Kaua‘i’s climate is strongly affected by its topography. During most of the year, trade winds blow from the northeast and are forced up the east-facing Wai‘ale‘ale escarpment near the center of the island. The rising air is confined near the island’s summit at 1593 m by a subsidence inversion at an elevation of 1.8-2.7 km (Ramage and Schroeder, 1999), which forces the air to drop much of its moisture at the summit. This produces a bulls-eye pattern in mean annual rainfall rates over the island, with high rainfall rates at the island’s center and low rainfall rates at the coast, superimposed upon a regional gradient with higher rainfall rates in the upwind northeastern half of the island than in the downwind southwestern half (Figure 2; PRISM Climate Group, Oregon State University). This results in one of the largest and steepest rainfall gradients on Earth. Rainfall rates between 1949 and 2004 on Mt. Wai‘ale‘ale near the island’s center averaged 9.5 m/yr – among the highest on Earth – while rainfall rates between 1949 and 2000 on the southwestern part of the island, just 25 km away, averaged 0.5 m/yr (Western Regional Climate Center). Given that a precipitation rate of 12.7 m/yr in Lloro, Colombia is often cited as the highest on Earth (e.g., Poveda and Mesa, 2000), the range of rainfall rates across Kaua‘i represents >70% of the range in rainfall rates on Earth. The wide range in rainfall rates and minimal variations in lithology make Kaua‘i an excellent natural laboratory for investigating the effects of rainfall rates on erosion rates.

METHODS: CALCULATING EROSION RATES

Million-year erosion rates inferred from basin excavation and bedrock age

A common method for estimating basin-averaged erosion rates E_V (M L^{-2} T^{-1}) is to measure the volume V of material of density ρ_r eroded from a basin of area A_b over a given time interval Δt, as in Equation 1.

$$E_V = \frac{\rho_r V}{A_b \Delta t} \qquad (1)$$

If the time interval Δt is taken to be the time between the construction of the initial topography and the present, this technique requires accurate estimates of the initial topography, the present topography, and the timing of the onset of erosion. This approach is amenable to application on young volcanic islands, because uneroded remnants of the volcano surface permit reconstruction of the pre-erosional volcano topography, and because many volcanic rocks are suitable for radiometric dating (e.g., Wentworth, 1927; Li, 1988; Ellen et al., 1993; Seidl et al., 1994; Hildenbrand et al., 2008).

Portions of Kaua‘i are suitable for such an approach. The western flank of Kaua‘i along the Na Pali Coast and above the Mana Plain, for example, is dissected with numerous drainage basins that are short (4-10 km from headwaters to outlet) and narrow (1-2 km wide). Rivers have incised narrow canyons into the centers of many of these drainage basins, and they have left relatively planar, minimally dissected topographic surfaces standing above and between many of the canyons, dipping toward the coast at gradients of 4-6°. The bedrock in this region is basalt of the Na Pali Formation, which is considered to be the remnant flank of Kaua‘i’s first volcanic edifice, and, with a K-Ar age of 4.43 ± 0.45 Ma, is the oldest dated bedrock on Kaua‘i (McDougall, 1979).

We used the minimally eroded interfluve surfaces in a 10-m digital elevation map (US National Elevation Dataset) to constrain the pre-erosional topography of each basin

along Kaua‘i’s western flank, similar to the approach that Seidl et al. (1994) and Stock and Montgomery (1999) used to estimate the vertical extent of river incision in the same region of Kaua‘i. For each basin, we constructed a model of the pre-erosional topography in two steps. First, we mapped the topography around the basin’s perimeter, including all neighboring remnants of minimally eroded topography and the basin ridgelines between the minimally eroded remnants. We then fit a thin-plate smoothing spline (with smoothing parameter $p = 1$, corresponding to a natural cubic spline) across the basin, fixing the edges of the spline surface to the mapped topography around the basin’s perimeter. Because the elevation of mapped perimeter may be as high as the initial topography but no higher, we consider the spline surface fit to the mapped perimeter to be a minimum bound on the elevation of the pre-erosional topography. We then subtracted the present topography from the initial topography to calculate the rock volume eroded from the basin, divided the eroded volume by the basin area and the age of the bedrock, and multiplied by an assumed rock density of $\rho_r = 3$ g/cm^3 to calculate a basin-averaged erosion rate (Equation 1; Table 1; Figure 2). We assume, in Equation 1, that uncertainties in drainage area, eroded volume, and bedrock density are negligible relative to the uncertainties in bedrock age (Table 1). This calculation does not include potential variations in basalt porosity, which would lower the bulk rock density and hence estimates of E_V.

Table 1: Basin-averaged erosion rates determined from rock volumes eroded since construction of the basin’s initial surface (Equation 1). ID refers to basin identification numbers in Figure 2. Values for mean annual precipitation (MAP)

are basin averages (Daly et al., 2002; PRISM Climate Group). Bedrock ages for lithologic units are: Na Pali formation 4.43 ± 0.45 Ma (McDougall, 1979); Olokele formation 3.95 ± 0.05 Ma (Clague and Dalrymple, 1988); Makaweli formation 3.91 ± 0.01 Ma (Clague and Dalrymple, 1988; Garcia et al., 2010); and Koloa volcanics in the Hanalei basin 1.50 ± 0.12 Ma (Clague and Dalrymple, 1988; Garcia et al., 2010).

Basin	ID	Area A_b (km^2)	Eroded volume V (km^3)	Bedrock age (Ma)	MAP (mm/yr)	Fraction f_V of initial volume eroded (%)	Erosion rate E_V (t km^{-2} yr^{-1})
Mana/Na Pali							
Awa‘awapuhi	1	2.70	0.154	4.43 ± 0.45	1337	5	36 ± 4
Haeleele	2	5.64	0.362	4.43 ± 0.45	1189	9	43 ± 4
Hanakapi‘ai	3	9.58	1.761	4.43 ± 0.45	3071	20	124 ± 13
Hanakoa	4	4.92	0.464	4.43 ± 0.45	2286	10	64 ± 6
Hikimoe	5	5.59	0.268	4.43 ± 0.45	1245	6	29 ± 3
Hoea	6	19.46	0.910	4.43 ± 0.45	841	8	30 ± 3
Honopu	7	3.29	0.613	4.43 ± 0.45	1187	20	124 ± 12
Huluhulunui	8	1.51	0.027	4.43 ± 0.45	639	7	11 ± 1
Kaawaloa	9	8.22	0.357	4.43 ± 0.45	918	7	29 ± 3
Kaaweiki	10	4.49	0.273	4.43 ± 0.45	1157	8	35 ± 4
Kahelunui	11	6.46	0.265	4.43 ± 0.45	913	6	25 ± 3
Kahoaloha	12	6.23	0.257	4.43 ± 0.45	1111	5	26 ± 3
Kalalau	13	10.45	3.633	4.43 ± 0.45	1479	33	217 ± 22
Kapilimao	14	4.13	0.129	4.43 ± 0.45	668	10	21 ± 2
Kauhao	15	7.62	0.793	4.43 ± 0.45	1280	12	64 ± 7
Ka‘ula‘ula	16	5.26	0.254	4.43 ± 0.45	1153	6	29 ± 3
Kuapa‘a	17	3.45	0.105	4.43 ± 0.45	707	9	21 ± 2
Makaha	18	6.40	0.477	4.43 ± 0.45	1269	8	44 ± 4
Miloli‘i	19	9.26	0.522	4.43 ± 0.45	1267	5	26 ± 3
Nahomalu	20	9.97	0.356	4.43 ± 0.45	1038	5	24 ± 2
Niu	21	2.83	0.108	4.43 ± 0.45	752	10	26 ± 3
Nu‘alolo	22	6.42	0.536	4.43 ± 0.45	1290	11	66 ± 7
‘Ohai‘ula	23	4.96	0.146	4.43 ± 0.45	899	6	20 ± 2
Paua	24	1.92	0.023	4.43 ± 0.45	654	5	8 ± 1
Wai‘aka	25	3.88	0.104	4.43 ± 0.45	688	8	17 ± 2
Wailao	26	3.15	0.110	4.43 ± 0.45	752	9	26 ± 3
Waipao	27	4.42	0.142	4.43 ± 0.45	720	8	22 ± 2
Large basins							
Hanalei	28	60.04	11.69 –	1.50 ± 0.12,	3866	32 – 42	175 – 309

			23.58	3.95 ± 0.05, 4.43 ± 0.45			
Hanalei (east)		21.42	1.56	1.50 ± 0.12, 4.43 ± 0.45	3301	19	146 ± 12
Hanalei (west)		38.62	10.13-22.02	3.95 ± 0.05, 4.43 ± 0.45	4179	39 – 55	192 – 400
Hanapepe	29	67.83	13.28	3.95 ± 0.05, 4.43 ± 0.45	2897	29	133 ± 13
Lumahai	30	35.63	15.78	3.95 ± 0.05, 4.43 ± 0.45	3716	45	335 ± 4
Makaweli	31	68.70	13.39	3.91 ± 0.01, 3.95 ± 0.05, 4.43 ± 0.45	2961	21	121 ± 3
Waimea	32	150.97	28.38	3.91 ± 0.01, 3.95 ± 0.05, 4.43 ± 0.45	1860	18	140 ± 3
Wainiha	33	58.29	23.86	3.95 ± 0.05, 4.43 ± 0.45	3909	36	303 ± 9

We calculated erosion rates for the six largest basins elsewhere on Kaua‘i – the Hanalei, Hanapepe, Lumahai, Makaweli, Waimea, and Wainiha basins – by the same general procedure, modified slightly to accommodate basins that contained multiple lithologies of distinct ages. That is, we divided each of these large basins into regions based on the mapped lithologies in Sherrod et al., 2007 (Figure 1), assigned each region an age based on published bedrock ages (Table 1), and calculated an erosion rate for each region. We then calculated basin-averaged erosion rates as the areally weighted mean of the sub-basin erosion rates.

Calculating the basin-averaged erosion rate for the Hanalei basin required one further step, because the east side and the west side of the Hanalei basin do not share a single initial topographic surface. The east side of the Hanalei basin dropped down relative to the west side some time after the Olokele caldera filled with lava (3.95 ± 0.05 Ma), and was subsequently blanketed with alkalic lava at 1.50 ± 0.12 Ma (Clague and Dalrymple, 1988; Sherrod et al., 2007; Garcia et al., 2010). It would therefore be

inappropriate to estimate the Hanalei basin's initial topography with a single spline surface. To account for the different structural histories in the east and west sides of the basin, we constructed independent spline surfaces for the east and west sides of the basin, calculated erosion rates for each side, and then calculated a basin-averaged erosion rate as the areally weighted mean of the two erosion rates. This exercise yielded a range of 175-309 t km^{-2} yr^{-1} for the Hanalei basin-averaged erosion rate, a range that primarily reflects uncertainties in the eroded volume in the western side of the basin where the initial topography is poorly constrained. The only remnant topography near the western side of the Hanalei basin is the central plateau west of the southern headwaters and the ~2 km^2 Namolokama plateau between the Lumahai and Hanalei basins (Figure 3). These plateaus constrain the initial elevation of the basin's western edge, but they do not constrain the initial topography between the basin's western edge and the Hanalei River. We therefore generated two spline surfaces to place upper and lower bounds on the initial topography of the western side of the Hanalei basin. The upper bound was created by fitting a spline surface to the Namolokama and central plateaus and extrapolating that nearly horizontal surface out over the western Hanalei basin. The lower bound was created by fitting a spline surface to the same plateaus plus the tributary ridgelines in the western Hanalei basin, which yielded a spline-fit surface that plunged down from the basin's high-altitude western edge to the present-day river. The upper- and lower-bound spline surfaces in the western Hanalei basin therefore yielded upper and lower bounds on the volume of rock that has been eroded, which in turn provide upper and lower bounds on erosion rates calculated with Equation 1.

Millennial erosion rates inferred from ^{3}He in detrital olivine

In basins where erosion proceeds at a steady incremental rate at the hillslope surface, basin-averaged erosion rates can be inferred from concentrations of cosmogenic nuclides in well-mixed stream sediment (Lal, 1991; Brown et al., 1995; Granger et al., 1996; Bierman and Steig, 1996). For cosmogenic ^{3}He (hereafter ^3He_c) in olivine, which is stable and produced through neutron spallation of Si, O, Mg, and Fe (Gosse and Phillips, 2001), the inferred erosion rate E_{3Hec} (M L^{-2} T^{-1}) is given by Eq. 2 (Lal, 1991).

$$E_{3Hec} = P_{3Hec}\Lambda/N \qquad (2)$$

Here P_{3Hec} (atoms g^{-1} yr^{-1}) is the production rate of ^3He_c at the hillslope surface, and is calculated at each site as a function of latitude and altitude following established procedures (Balco et al., 2008; Goehring et al., 2010). The attenuation constant Λ (160 ± 10 g cm^{-2}; Gosse and Phillips, 2001) is an empirical constant that describes the exponential attenuation of the cosmogenic neutron flux as it passes through matter, and N (atoms/g) is the concentration of ^3He_c in olivine, with uncertainties derived from multiple helium measurements on aliquots of the same sample. Erosion rates inferred from ^3He_c concentrations are averaged over the characteristic timescale of ^3He_c accumulation, Λ/E_{3Hec}. For an erosion rate of 160 t km^{-2} yr^{-1}, for example, this characteristic timescale would be 10,000 years.

We use Equation 2 to constrain millennial-scale erosion rates in the Hanalei basin, the only basin on Kaua‘i where fluvial sediment flux measurements provide a reliable estimate of modern erosion rates against which millennial-scale erosion rates may be compared. We collected stream sediment samples at the site of the USGS gauging station in the Hanalei River (USGS gauge 16103000) and in four of the Hanalei River’s

tributaries (Figure 3). After air drying sediment samples, olivine grains were hand-picked under a microscope from the 0.520-4.76 mm size fraction for helium analysis. One of the sediment samples (HAN020A) was composed of pebbles <32 mm, which themselves were composed of a basalt matrix containing olivine phenocrysts, and we crushed the pebbles in this sample to the same 0.520-4.76 mm grain size to free olivines from the matrix. The other four sediment samples were sand-sized and contained abundant free olivine grains and were not crushed before olivine picking. Olivine grains were leached in a solution of 1% oxalic acid and 1% phosphoric acid at 80 °C for two hours, rinsed, dried, and then air-abraded for 15-20 minutes. The purpose of these steps was to remove the outer 20-30 mm of the grains that may have implanted ^{4}He from U and Th decay occurring outside the olivine grains in the basalt matrix.

The total ^{3}He concentration in an olivine grain collected at the Earth's surface is the sum of $^{3}He_c$, magmatic ^{3}He, and nucleogenic ^{3}He. Nucleogenic ^{3}He is produced in olivine by reaction of lithium with epithermal neutrons ($^{6}Li + n \rightarrow {}^{3}H + \alpha$) followed by radioactive decay of tritium ($^{3}H \rightarrow {}^{3}He + \beta$; $t_{1/2} = 12$ yr; Andrews et al., 1982). Nucleogenic ^{3}He concentrations in the Hanalei olivines will, however, be quite low ($\leq 2 \times 10^{4}$ at/g) due to the low abundance of Li in the olivines ($\leq$2 ppm; Table 2). On the other hand, magmatic ^{3}He ($^{3}He_{magmatic}$) trapped in melt and fluid inclusions is frequently the dominant source of ^{3}He within the olivine crystal. If $^{3}He_{magmatic}$ in the olivine crystals can be determined and nucleogenic ^{3}He is negligible, then $^{3}He_c$ can be calculated. We attempted to calculate $^{3}He_c$ concentrations using standard laboratory procedures (e.g., Kurz, 1986); details of the analytical techniques have been published previously (Gayer et al., 2008). First, we crushed olivine grains under vacuum, which only releases the

magmatic He trapped in the melt and fluid inclusions and thereby allows us to determine the magmatic $^3He/^4He$ ratio. The crushed powders were then fused in a furnace, which liberates ^3He_c, $^3He_{magmatic}$, magmatic ^4He and radiogenic ^4He. Here magmatic ^4He is the ^4He trapped in olivine during crystallization from the magma, and radiogenic ^4He is the amount of ^4He that accumulated in the olivines from decay of U, Th and ^{147}Sm since the olivines cooled below the closure temperature of He in olivine.

The ^3He_c concentrations can then be related to the amount of He released during the furnace step ($^3He_{furnace}$) through the following equations:

$$^3He_c = {}^3He_{furnace} - {}^3He_{magmatic} - {}^3He_{nucleogenic} \quad (3)$$

and

$$^3He_{magmatic} = ({}^4He_{furnace} - {}^4He_{radiogenic})\,({}^3He/{}^4He)_{crush}. \quad (4)$$

We computed the concentrations of radiogenic ^4He from measurements of U, Th, and Sm concentrations in the olivine aliquots by ICP-MS (Table 2), which yielded estimates of $^3He_{magamtic}$ through Equation 4. However, in each of our samples, the calculated $^3He_{magmatic}$ concentration is larger than the measured $^3He_{furnace}$ concentration, indicating that the calculated concentrations of $^3He_{magmatic}$ are too large. This in turn indicates that the radiogenic ^4He concentrations computed from the U-Th-Sm concentrations in the olivines are too low compared to the actual amount of radiogenic ^4He released on fusing the olivine powders. Understanding the source of the additional radiogenic ^4He in the olivine crystals will require additional research. For the present study, we used the ^3He content measured by fusing the olivine powders ($^3He_{furnace}$) as an upper bound on ^3He_c (Equation 3). Since ^3He_c is inversely related to erosion rates (Equation 2), the upper bounds on ^3He_c provide minimum bounds on erosion rates. In

calculating minimum bounds for E_{3Hec}, we used values for basin-averaged P_{3He} calculated with the Lal/Stone scaling in the CRONUS calculator (Balco et al., 2008) assuming a sea-level high-latitude production rate of 121 ± 11 atoms g^{-1} yr^{-1} (Goehring et al., 2010), and with topographic shielding corrections calculated at each pixel in a 10-meter DEM of the basin (Niemi et al., 2005; Balco et al., 2008; Gayer et al., 2008).

We note that calculating basin-averaged erosion rates with Equation 2 carries an implicit assumption that olivine abundances in the material supplied to the channel network are spatially constant throughout the basin upstream of the sediment sampling site (e.g., Bierman and Steig, 1996). We were unable to validate this assumption in the Hanalei basin because much of the basin is difficult to access on foot, which limited our field observations to channels and low-altitude ridgelines. In the field we observed abundant olivine grains up to 3 mm in diameter in stream sediment at each of the sample sites, which indicates that at least a portion of the underlying basalt in each of the sampled basins contributed olivine grains to the channel network. We also observed that soils on two low-altitude ridgelines in the northwestern Hanalei basin are olivine-poor, which suggests that in these low-altitude basins, olivines might be delivered to the channel primarily from non-soil sources, such as from slowly exhumed corestones, which we also observed on the same ridgelines. Thus we do not argue that the supply of olivines to the channel network is constant in space within each sampled basin; our field observations are too limited in space to draw definitive conclusions about this. Validating that argument will require measuring olivine abundances in hillslope material throughout the Hanalei basin, including its high-gradient, high-altitude terrain. In this analysis, we applied Equation 2 under the assumption that olivine abundances are

spatially constant throughout the basin, and note that future determination of olivine sources within the Hanalei basin will permit reinterpretation of measured cosmogenic nuclide concentrations.

Table 2: Characteristics of detrital olivine samples for ^{3}He analysis (Figure 3). Latitude, longitude, and elevation indicate sites of stream sediment sampling, while bedrock age, mean hillslope gradient, mean annual precipitation (MAP), and cosmogenic ^{3}He production rates (P_{3He}) are means over the contributing basins. Values for basin-averaged P_{3He} were calculated with the Lal/Stone scaling in the CRONUS calculator (Balco et al., 2008) assuming a sea-level high-latitude production rate of 121 ± 11 atoms g^{-1} yr^{-1} (Goehring et al., 2010), with topographic shielding corrections calculated at each pixel in a 10-meter DEM of the basin, following Niemi et al. (2005), Balco et al. (2008) and Gayer et al. (2008). Concentrations of ^{7}Li, ^{238}U, ^{232}Th, and ^{147}Sm were measured by ICP-MS on aliquots of olivine grains, and were used to calculate concentrations of radiogenic ^{4}He ($^4He_{rad}$; e.g., Farley, 2002). Values of n are the number of olivine grains used in each analysis, and values of R/R_A are the measured ^{3}He/^{4}He ratios (R) normalized by the atmospheric ^{3}He/^{4}He ratio ($R_A = 1.39 \cdot 10^{-6}$). Values of $^3He_{magmatic}$ were calculated with Equation 3 and 4 using $(^3He/^4He)_{crush}$, the calculated value of $^4He_{rad}$, and the measured concentrations of $^4He_{furnace}$. Minimum bounds on inferred erosion rates (Min. E_{3Hec}) were calculated with Equation 2 by taking $^3He_{furnace}$ to be an upper bound on $^3He_{cosmogenic}$. Uncertainties on Min. E_{3Hec} were calculated by propagating uncertainties in P_{3He} , $^3He_{furnace}$, and the attenuation length scale $\Lambda = 160 \pm 10$ g/cm^2 (Gosse and Phillips, 2001). Values marked n/d were not determined.

	Sampling sites							Isotopic concentrations in olivine					
Sample	Latitude (°N)	Longitude (°W)	Elev. (m)	Rock age (Ma)	Mean slope (°)	MAP (m/yr)	Mean ± s.e. P_{3He} (at g^{-1} yr^{-1})	Mass (g)	^{7}Li (ppm)	^{238}U (ppb)	^{232}Th (ppb)	^{147}Sm (ppb)	$^4He_{rad}$ (10^9 at/g)
HAN003	22° 5' 31.23"	159° 28' 55.92"	468	4.02	38.6	6.62	163 ± 15	0.1014	1.89	0.167	0.449	4.262	4.01
HAN006	22° 5' 24.81"	159° 28' 24.34"	389	4.00	44.0	6.94	150 ± 14	0.0787	1.90	0.303	0.754	8.281	7.10
HAN011	22° 9' 28.81"	159° 28' 25.67"	81	3.95	35.9	3.44	105 ± 10	n/d	n/d	n/d	n/d	n/d	n/d
HAN017	22°10' 46.62"	159° 27' 58.75"	23	3.04	31.3	4.26	115 ± 10	0.1017	1.87	0.184	0.408	5.384	3.20
HAN020A	22° 9' 12.05"	159° 28 '19.12"	81	3.85	43.8	4.07	112 ± 10	0.1003	1.97	0.439	1.108	10.329	9.78

	Helium measurements during crush					Helium measurements during heating (mean ± s.e. of two analyses)						
Sample	Mass (g)	n	^{3}He (10^6 at/g)	^{4}He (10^{10} at/g)	R/R_A	Mass (g)	n	$^3He_{furnace}$ (10^5 at/g)	$^4He_{furnace}$ (10^{10} at/g)	R/R_A	$^3He_{magmatic}$ (10^5 at g^{-1})	Min. E_{3Hec} (t km^{-2} yr^{-1})
HAN003	0.360	54	5.26	15.8	23.9	0.2134 ± 0.1073	99 ± 46	6.69 ± 0.09	2.48 ± 0.31	19.4 ± 2.4	6.91 ± 1.03	390 ± 43
HAN006	0.398	77	2.61	6.84	27.5	0.2008 ± 0.0024	156 ± 79	18.17 ± 6.71	9.01 ± 0.54	14.5 ± 5.4	31.68 ± 2.08	132 ± 51
HAN011	0.388	104	21.8	64.7	24.3	0.2400 ± 0.0180	130 ± 26	10.18 ± 1.47	7.53 ± 3.30	9.7 ± 4.5	n/d	165 ± 30
HAN017	0.400	101	16.5	42.9	27.7	0.2569 ± 0.0008	167 ± 66	7.77 ± 1.66	5.36 ± 2.37	10.4 ± 5.1	19.42 ± 9.12	238 ± 57
HAN020A	0.389	123	9.99	27.0	26.6	0.2456 ± 0.0134	212 ± 89	14.24 ± 1.99	5.00 ± 0.53	20.5 ± 3.6	14.88 ± 1.97	126 ± 22

Modern erosion rates inferred from fluxes of sediment and solutes

Basin-wide erosion rates can also be measured by monitoring the flux of rock-derived material out of a river and via groundwater discharge to the ocean. With the exception of a one-year gap from 1 October 2006 to 30 September 2007, suspended sediment fluxes E_{ss} (M L^{-2} T^{-1}) in the Hanalei River were measured daily from 1 October 2003 to 30 September 2009 by the United States Geological Survey at USGS gauge 16103000, four km southeast of the town of Hanalei (Figure 3; USGS National Water Information System). These data permit calculation of a mean and standard error for the annual suspended sediment flux.

The suspended sediment flux is, of course, only a portion of the total mass flux E_{efflux} from the Hanalei basin. Additional mass is lost from the basin as fluvial bedload at a rate E_{bed}, as fluvial solutes at a rate E_{wf}, and as solutes in groundwater discharging directly to the ocean at a rate E_{ws}.

$$E_{\mathrm{efflux}} = E_{\mathrm{ss}} + E_{\mathrm{bed}} + E_{\mathrm{wf}} + E_{\mathrm{ws}} \qquad (5)$$

Neither solute fluxes nor bedload fluxes were monitored in the Hanalei basin during 2003-2009. Previous measurements, however, permit estimation of solute fluxes in the Hanalei basin. We estimate E_{wf} from Hanalei River solute flux measurements between 1971 and 1976 (Dessert et al., 2003), and we take Li's (1988) estimate of Kaua‘i-averaged subsurface solute fluxes as representative of E_{ws} in the Hanalei basin. Because neither Dessert et al. (2003) nor Li (1988) reported uncertainties on their estimates of solute fluxes, we conservatively assign uncertainties of 50% of the mean flux for each of E_{wf} and E_{ws}. In the absence of bedload flux measurements in the Hanalei basin or elsewhere on Kaua‘i, we tentatively take bedload fluxes at the Hanalei gauging

station to be 10% of the physical sediment flux, a ratio that is commonly applied in other rivers (e.g., Dietrich and Dunne, 1978). To be conservative, we further assume that the uncertainty on the bedload flux is half of the mean bedload flux. That is, we assume that $E_{\mathrm{bed}} = (0.1 \pm 0.05)E_{\mathrm{ss}}$. We emphasize that bedload to suspended load ratios can differ substantially among different rivers (e.g., Turowski et al., 2010), and that the true bedload to suspended load ratio in the Hanalei River is unconstrained by measurements. Future bedload flux measurements in the Hanalei River will be required to provide a basis for revising the assumed ratio.

Modern erosion rates due to shallow landslides

The rate of erosion due to landslides, E_L (M L^{-2} T^{-1}), can be calculated by summing the eroded mass of landslide-derived material over a known area A and dividing by the time interval Δt during which the landslides occurred (e.g., Hovius et al., 1997).

$$E_L = \frac{\sum_{i=1}^{n} \rho V_i}{A \Delta t} \qquad (6)$$

Here n is the number of landslides that occurred over Δt, ρ (M/L^3) is the density of eroded material, and V_i (L^3) is the volume of the ith landslide. Because Equation 6 implicitly assumes that all material eroded by a landslide is delivered to a channel, it yields an upper bound on short-term landslide-derived erosion rates.

Our field observations of steep hillslopes in Kaua‘i’s Hanalei River basin suggest that shallow landslides are common and may be an important component of hillslope mass fluxes (Figure 4). We use Equation 6 to estimate landslide-derived physical erosion rates by mapping landslide scars in repeat satellite images of the Hanalei basin (Figure 5;

Table 3). The first of these is a mosaic of two 0.6 m/pixel QuickBird satellite images acquired on 5 January 2004 and 14 October 2004, stitched together to ensure coverage of the entire Hanalei basin. The second image, with a pixel size of 0.5 m, was acquired by the WorldView-2 satellite on 2 January 2010. Because >94% of the landslide scars visible in the QuickBird mosaic appear in the 5 January 2004 image, we apply a Δt corresponding to the time difference between 5 January 2004 and 2 January 2010 (5.99 years) in Equation 6. This interval is close to the span of the USGS suspended sediment flux measurements, which extends from 1 October 2003 to 30 September 2009.

Table 3: Statistics of satellite imagery and mapped landslide scars. Values of n are estimates of the maximum and minimum bounds on the number of landslide scars in the mapped area. Estimates of landslide physical erosion rate E_L (Equation 6) and landslide frequency f_L are based on the number of new landslide scars in the WorldView-2 image relative to the QuickBird image.

Image	Dates	Resolution (m/pixel)	Spectral bands used in mapping	Visible basin area A (km^2)	Number of mapped scars
QuickBird mosaic	2004/1/5, 2004/10/14	0.6	RGB, near-IR	52.80	285 – 697
WorldView-2	2010/1/2	0.5	RGB, near-IR	49.65	142 – 286

Time interval	Number of new scars n	New scar area (m^2)	New scar volume (m^3)	Mappable area A (km^2)	f_L (scars km^{-2} yr^{-1})	E_L (t km^{-2} yr^{-1})
2004-2010	36-62	10,205 - 13,733	9023 - 11,747	48.21	0.12 – 0.22	30 – 47

We examined the QuickBird and WorldView-2 images at 1:1000 scale using their visible (red, green, blue) and near-infrared wavelengths, and mapped features that we

considered to be landslide scars in both images (Figure 5). This procedure for mapping landslide scars carries with it some ambiguity. Although young scars are easily identifiable by their sharp edges and red-brown color, many older scars are partially revegetated, which in satellite imagery blurs the edges of scars and makes the color of scars a mixture of red-brown and green. This makes it difficult to definitively identify features in satellite images as landslide scars. This difficulty is most pronounced for small scars, which are common in the Hawaiian Islands. Peterson et al. (1993) and Ellen et al. (1993), for example, reported mapping landslide scars on Oahu as small as 10 m^2, which at the resolution of the QuickBird satellite image could be as small as 5 by 6 pixels.

To address the ambiguity inherent in identifying landslide scars in satellite imagery, we report two sets of landslide scar statistics to put upper and lower bounds on inferred landslide-derived erosion rates. We did so by classifying the mapped landslide scars as "most certain" or "less certain," based on the feature's color and the sharpness of the boundary between the feature and its surroundings. Although this classification is subjective, it permits identification of features that we consider most likely to be landslide scars, which permits estimation of upper and lower bounds on the number of landslide scars and hence landslide-derived erosion rates.

Due to the large number of landslide scars and the inaccessibility of much of the study area, we were unable to measure the volume of each landslide scar in the field. Instead, we measured each scar's planform area A_L in the satellite images and estimated its volume V from an empirical relationship between volume and area in a global inventory of soil-based landslide scars ($V = \alpha A_L^b$, with best-fit values of $\log(\alpha) = -0.44 \pm$

0.02 (mean ± s.e.) and b = 1.145 ± 0.008 (mean ± s.e.); n = 2136; Larsen et al., 2010). In our application of Equation 6, we assumed negligible uncertainties in Δt, ρ, and A.

Table 4: Sources of uncertainty in erosion rate estimates

Method	Sources of uncertainty
Basin volume E_V (Eq. 1)	Bedrock ages (Table 1; McDougall, 1979; Clague and Dalrymple, 1988; Garcia et al., 2010) Bedrock density (uncertainty assumed negligible) Eroded volumes (uncertainties assumed negligible) Drainage areas (uncertainties assumed negligible)
^{3}He-based E_{3Hec} (Eq. 2)	Production rate P_{3Hec} (Table 2; Goehring et al., 2010) Attenuation constant Λ (Table 2; Gosse and Phillips, 2001) ^{3}He concentrations (Table 2; s.e. of two measurements)
Modern fluxes E_{efflux} (Eq. 5)	E_{ss} (Mean flux from USGS suspended sediment flux monitoring, 2003-2009; uncertainty is s.e. of annual fluxes, which yields 369 ± 114 t km^{-2} yr^{-1}.) E_{bed} (Mean flux assumed to be 10% of suspended sediment flux; uncertainty assumed to be 50% of mean flux, which yields 37 ± 18.5 t km^{-2} yr^{-1}.) E_{wf} (Mean flux from Dessert et al., 2003; uncertainty assumed to be 50% of mean flux, which yields 102 ± 51 t km^{-2} yr^{-1}.) E_{ws} (Mean flux from Li, 1988; uncertainty assumed to be 50% of mean flux, which yields 37 ± 18.5 t km^{-2} yr^{-1}.)
Landslide E_L (Eq. 6)	Scar volumes (area-volume scaling relationship $V = \alpha A_L^b$, with log(α) = -0.44 ± 0.02 (mean ± s.e.) and b = 1.145 ± 0.008 (mean ± s.e.); Larsen et al., 2010) Soil density (field measurement; uncertainty assumed negligible) Basin area (uncertainty assumed negligible) Timespan between satellite images (uncertainty assumed negligible)

RESULTS AND DISCUSSION

Spatial patterns in Myr-scale erosion rates and precipitation rates across Kaua‘i

Two main observations can be drawn from the pattern of Myr-scale erosion rates across Kaua‘i in Figure 2. First, basin-averaged erosion rates E_V vary by more than a factor of 40 across the island, from as high as 335 t km^{-2} yr^{-1} to as low as 8 t km^{-2} yr^{-1}, with the lowest rates along the island’s west flank, the highest rates on the island’s north side, and intermediate rates in the large canyons draining to the south. These Myr-scale erosion rates are positively correlated with modern basin-averaged mean annual

precipitation rates, consistent with a positive influence of precipitation rates on erosion rates (Figure 2B). Considering the absence of strong correlations between erosion rates and precipitation rates in several other compilations, (e.g., Walling and Webb, 1983; von Blanckenburg, 2005; Portenga and Bierman, 2011), this correlation is striking. This correlation may be more apparent on Kaua‘i than elsewhere because the study basins have such a large range in precipitation rates but only small variations in potentially confounding factors like lithology and rock uplift rate. We stress, however, that this correlation is only coarsely indicative of how rainfall rates should affect landscape evolution, because estimates of E_V do not reveal which erosional processes are active or how sensitive each process is to rainfall rates. Indeed, the dominant processes of erosion have likely changed over Kaua‘i’s lifespan, since mass fluxes on very young volcanic islands tend to be dominated by subsurface chemical weathering fluxes (e.g., Rad et al., 2007; Schopka and Derry, 2012), while on older islands the dominant mass transport processes shift to bedrock river incision, soil creep, and landsliding (e.g., Wentworth, 1943; Lamb et al., 2007). Ultimately, incorporating the effects of precipitation rates into landscape evolution models will require quantifying how precipitation rates influence the rate coefficients for specific erosion processes like bedrock river incision and hillslope soil production and transport. In the final section of this paper, we consider the implications of our measurements for large-scale relationships between climate, erosion, and tectonics.

The second main observation in Figure 2 concerns the extent of basin excavation f_V, which we define as the ratio of the eroded rock volume to the initial rock volume that was available to be eroded before erosion began – i.e., the volume of an imaginary wedge

defined by the basin's present-day lateral boundaries, the initial topographic surface, and sea level. This ratio can be thought of as the basin's fractional volume loss. It is useful because it is less sensitive than E_V to differences among basins in the local topography and thickness of the initial shield surface. That is, because E_V is calculated by dividing eroded volumes by basin area (Equation 1), E_V may be partly dependent on the vertical thickness of rock that existed between the initial topographic surface and sea level, simply because more volume per unit basin area can be eroded from a thick wedge of rock than from a thin wedge. Because some basins on Kaua'i had larger initial thicknesses than others, the estimates of E_V in Figure 2 may partly reflect differences in initial topography among basins, which may obscure the effects of climate on the efficiency of basin erosion. Calculating f_V, by contrast, involves normalizing eroded volumes by initial basin volume, which yields a measure of basin excavation that is independent of the basin's initial topography. As Figure 2C shows, the extent of basin excavation is positively correlated with modern mean annual precipitation rates above precipitation rates of ~1 m/yr. Together, Figures 2B and 2C show that wetter basins have higher Myr-scale erosion rates than drier basins do, and that wetter basins have lost a larger fraction of their initial rock volume than drier basins have.

Although most basins in Figure 2 lie along a power-law trend between erosion rate and mean annual precipitation, three basins draining to the Na Pali coast – Honopu, Hanakapi'ai, and Kalalau – lie above this trend. To the extent that Figure 2 implies that Myr-scale erosion rates ought to scale with mean annual precipitation, the deviation of these points from the trend suggests that these basins eroded anomalously quickly for their climatic settings relative to the other basins on Kaua'i. One possible explanation for

the high erosion rates in these three basins is rapid knickzone retreat initiated by flank failure on the Na Pali coast. Some studies have interpreted the existence of large knickzones in rivers draining to the Na Pali coast (and the absence of knickzones in similarly sized basins draining to Kaua‘i’s west coast) as evidence for a propagating wave of incision initiated by a massive flank failure on the Na Pali coast (e.g., Moore et al., 1989; Seidl et al., 1994; Stock and Montgomery, 1999), similar to the suggestion that a flank failure initiated a wave of incision on Hawaii’s Kohala coast (Lamb et al., 2007). Although our basin-averaged erosion rate measurements cannot confirm the occurrence or timing of a flank failure along the Na Pali coast, a rapidly propagating wave of river incision through the channel networks would have accelerated erosion of the neighboring hillslopes and generated erosional patterns that would be consistent with the erosional patterns in Figure 2.

The basin-averaged precipitation rates in Figure 2 are inferred from rainfall measurements made over the past few decades (Daly et al., 2002; PRISM Climate Group, Oregon State University), an interval that is far shorter than the ~4 Myr associated with the basin-averaged erosion rates. This difference in timescales is important because spatial patterns in precipitation rates may have differed in the past, which would mean that Kaua‘i’s topography evolved to its present state under a time-varying climate that differed from the present climate. For instance, precipitation rates may have varied in response to changes in regional climate, changes in the elevation of the atmospheric temperature inversion, and changes in the island’s topography as it subsided and was carved by rivers (e.g., Hotchkiss et al., 2000; Chadwick et al., 2003). Thus the degree to which spatial patterns in modern precipitation rates are representative of spatial patterns

in paleoprecipitation rates depends on the degree to which the factors that controlled paleoprecipitation rates – i.e., the dominant wind direction and the elevation of the topography relative to that of the atmospheric inversion – were similar to those factors today.

Unfortunately, there is only limited observational evidence to constrain past wind conditions and the paleoelevation of Kaua‘i relative to the atmospheric inversion over the past 5 Myr (e.g., Gavenda, 1992). The orientation of lithified sand dunes (Stearns, 1940; Stearns and Macdonald 1942; 1947; Macdonald et al., 1960; Porter, 1979) and the asymmetry of pyroclastic cones (Wentworth, 1926; Winchell, 1947; Porter, 1997) elsewhere in the Hawaiian Islands suggest that regional winds during glacial periods were dominated by northeasterly trade winds, as they are today. The existence of submarine terraces encircling Kaua‘i have been interpreted as an indication that Kaua‘i has subsided 800-1400 m since submersion of the terraces (Mark and Moore, 1987; Flinders et al., 2010). There are no quantitative constraints on the atmospheric inversion layer altitude over time, but palynological evidence on Oahu suggests that low- to mid-elevation windward sites received more precipitation during glacial periods than at present, which has been interpreted as an indication that the inversion layer was lower during glacial periods than at present (Hotchkiss and Juvik, 1999). These observations suggest that a portion of Kaua‘i may have spent some time above the atmospheric temperature inversion over the past 4-5 Myr, given that (1) the modern elevation of the atmospheric temperature inversion fluctuates between ~1800 m and ~2700 m (Ramage and Schroeder, 1999); (2) Kaua‘i’s highest point is currently at an elevation of 1593 m; (3) Kaua‘i was likely 800-1400 m higher before subsidence; and (4) the atmospheric inversion was likely

at lower altitudes during glacial periods. If this is true, then the portion of the island above the temperature inversion may have been drier than sites below the inversion, and the spatial pattern of precipitation rates across Kaua‘i may have differed from that at present.

Hotchkiss et al. (2000) attempted to account for changes in topography, regional climate, and the atmospheric inversion altitude in a model of soil development at one site on Kaua‘i’s Kokee ridge, and concluded that the mean annual precipitation rate at that site over the past 4.1 Myr was roughly 87% of the present-day mean annual precipitation rate, which suggests that modern rainfall rates may be similar to those over the past 4.1 Myr. To the extent that their model is accurate and Kokee Ridge is representative of Kaua‘i as a whole, this model result suggests that modern precipitation rates may be a reasonable proxy for the paleoprecipitation rates that influenced Kaua‘i’s topographic evolution.

Irrespective of how spatial patterns in precipitation rates across Kaua‘i have evolved over the past 4-5 Myr, there remains a positive correlation between the Myr-scale basin-averaged erosion rates in Figure 2B and modern basin-averaged precipitation rates. Such a strong correlation would be surprising if spatial patterns in paleoprecipitation rates were very different from those at present. If that were the case, the correlation in Figure 2B would imply that erosion rates were controlled by factors other than mean annual precipitation that fortuitously covaried with modern mean annual precipitation. There are, however, no obvious non-climatic factors (e.g., lithology, rock uplift rates) that covary with mean annual precipitation across Kaua‘i and which might strongly affect erosion rates. We acknowledge that it is possible that other moments of

precipitation, such as storminess, might also covary with mean annual precipitation and might influence long-term erosion rates (e.g., DiBiase and Whipple, 2011), but the simplest explanation for the correlation in Figure 2B is a dependence of erosion rates on mean annual precipitation.

Modern, million-year, and millennial erosion rates in the Hanalei basin

Annual suspended sediment discharges at the Hanalei River monitoring station (USGS gauge 16103000) between 2003 and 2009 range from 153 t km^{-2} yr^{-1} to 690 t km^{-2} yr^{-1}, with a mean and standard error of E_{ss} = 369 ± 114 t km^{-2} yr^{-1}. Dessert et al. (2003) reported 1971-1976 USGS measurements of runoff (3.6 m/yr) and total dissolved solids (28.3 mg/l) in the Hanalei River, which imply a fluvial solute flux of 102 t km^{-2} yr^{-1}. In the absence of measurements on atmospheric solute inputs or changes in intra-basin solute storage over the same time period, we take this to be representative of the fluvial chemical erosion rate E_{wf}. Li (1988) estimated that groundwater discharge to the ocean is responsible for an additional E_{ws} = 37 t km^{-2} yr^{-1} of subsurface solute losses across Kaua‘i, calculated as the product of the island-average groundwater recharge rate and the mean chemical composition of groundwater. For the purposes of estimating the total mass flux in the Hanalei basin, we tentatively assume that fluvial solute fluxes in the Hanalei basin in 2003-2009 were comparable to those in 1971-1976, and that subsurface chemical erosion rates in the Hanalei basin match the island-wide subsurface chemical erosion rate in Li (1988). This is an approximation. Fluvial solute fluxes between 2003 and 2009 might have differed from those between 1971 and 1976, and subsurface solute fluxes from the Hanalei basin (which is wetter than most basins on Kaua‘i) might differ

from island-average subsurface solute fluxes. Neither Dessert et al. (2003) nor Li (1988) reported uncertainties on the reported solute fluxes, despite a number of potential sources of error in the determination of fluvial and subsurface solute fluxes (e.g., uncertainties in evapotranspiration rates, atmospheric solute deposition rates, and short-term changes in solute storage in biota or the subsurface). To be conservative, we apply 50% uncertainties to both the fluvial and subsurface solute flux estimates, and calculate the Hanalei basin's total chemical erosion rate as $E_{wf} + E_{ws} = (102 \pm 51\ \mathrm{t\ km^{-2}\ yr^{-1}}) + (37 \pm 18.5\ \mathrm{t\ km^{-2}\ yr^{-1}}) = 139 \pm 54\ \mathrm{t\ km^{-2}\ yr^{-1}}$.

These estimates can be compared with Kaua'i-wide estimates of surface and groundwater fluxes of dissolved silica and total alkalinity (Schopka and Derry, 2012). We convert Schopka and Derry's reported fluxes from mol/yr to t km^{-2} yr^{-1} using the area of Kaua'i (1437 km^2), a molar mass of 60.08 g/mol for silica, and an average molar mass of 63.1 g/mol for total alkalinity (i.e., the average molar mass of the oxides of the major cations that balance the charge in the total alkalinity (Na_2O, K_2O, CaO, and MgO)). With this conversion, we calculate that Schopka and Derry's Kaua'i-wide estimates of surface solute fluxes ($68 \pm 20\ \mathrm{t\ km^{-2}\ yr^{-1}}$) and groundwater solute fluxes ($33 \pm 9\ \mathrm{t\ km^{-2}\ yr^{-1}}$) agree with our estimates within uncertainty, which suggests that our estimates of solute fluxes in the Hanalei basin are of reasonable magnitude. In the absence of empirical constraints on bedload fluxes in the Hanalei basin or elsewhere on Kaua'i, we tentatively take bedload fluxes at the Hanalei gauging station to be 10 ± 5% of the physical sediment flux, for a physical sediment flux of $E_{ss} + E_{bed} = (369 \pm 114\ \mathrm{t\ km^{-2}\ yr^{-1}}) + (0.1 \pm 0.05)(369 \pm 114\ \mathrm{t\ km^{-2}\ yr^{-1}}) = 406 \pm 116\ \mathrm{t\ km^{-2}\ yr^{-1}}$. Combining these estimates yields a

total mass flux of E_{efflux} = (406 ± 116 t km^{-2} yr^{-1}) + (139 ± 54 t km^{-2} yr^{-1}) = 545 ± 128 t km^{-2} yr^{-1} from the Hanalei basin.

Because suspended sediment fluxes were monitored in the Hanalei basin only from 2003 to 2009, it is not possible to directly quantify how representative sediment fluxes during this period were relative to those during the previous decades. However, water discharges measured in the Hanalei River during 58 years of monitoring up to the present suggest that the basin did not experience unusually intense storms during the 2003-2009 period (USGS National Water Information System). The Hanalei River's largest peak discharge during the 2003-2009 monitoring period occurred in February 2006, and it had an intensity that is exceeded by 19 floods during the 58 years on record, including two floods that occurred after suspended sediment monitoring ended in 2009. Thus, the Hanalei River's hydrologic monitoring record suggests that the largest floods between 2003 and 2009 were not unusually large relative to floods before or since, which in turn suggests that our estimates of Hanalei mass fluxes during this interval are unlikely to be skewed high by the 2006 storm event.

These calculations suggest that modern mass fluxes from the Hanalei basin (545 ± 128 t km^{-2} yr^{-1}) are at least 1.8 ± 0.5 and at most 3.1 ± 0.8 times faster than mass fluxes from the Hanalei basin averaged over the past several million years (which have minimum and maximum bounds of 175 t km^{-2} yr^{-1} and 309 t km^{-2} yr^{-1}, respectively; Table 1). By comparison, minimum bounds on kyr-scale erosion rates E_{3Hec} based on ^{3}He concentrations in detrital olivine range from >126 to >390 t km^{-2} yr^{-1} (Table 2). As described in the Methods section, these are minimum bounds on erosion rates because they rest on the assumption that all the measured ^{3}He is cosmogenic. These erosion rates

may be considered averages over characteristic timescales Λ / E_{3Hec} of <12.7 kyr to <4.1 kyr, respectively.

These estimates of E_{3Hec} differ among tributary basins by a factor of three, which we suggest is not large; such differences in cosmogenically-inferred erosion rates are common among small tributary basins (e.g., Ferrier et al., 2005). The basin-to-basin differences in E_{3Hec} may reflect inter-basin differences in erosion rates or radiogenic ^{4}He concentrations, or they may reflect intra-basin variability in ^{3}He concentrations and the relatively small number ($n \sim 100$) of olivine grains in the samples in which ^{3}He concentrations were measured (e.g., Gayer et al., 2008). These minimum bounds on millennial-scale erosion rates bracket the only other basin-averaged erosion rates inferred from detrital ^3He_c on Kaua‘i (168 t km^{-2} yr^{-1} in the Waimea River; Gayer et al., 2008), and are similar to the estimates of Myr-scale erosion rates in the Hanalei basin and the Waimea basin (Table 1). The measured ^{3}He concentrations offer no upper bounds on kyr-scale erosion rates, but the minimum bounds on E_{3Hec} are consistent with the possibility that erosion rates in the Hanalei basin over the past few thousand years were comparable to erosion rates in the Waimea basin over the past few thousand years, as well as to erosion rates in the Hanalei basin over the past few million years.

The most relevant ^{3}He-based erosion rate to compare to modern stream sediment fluxes is the rate of >238 t km^{-2} yr^{-1} at site HAN017 (Figure 3), because this sample was collected at the site of the USGS Hanalei River gauging station and therefore averages over the same drainage area (47.9 km^2 of the Hanalei basin’s total drainage area of 60.0 km^2) as the modern suspended sediment fluxes do. What fraction of the modern mass flux should the ^{3}He-based erosion rates be compared to? Erosion rates inferred from ^3He_c

concentrations are representative of mass losses over the characteristic depth of ^3He_c accumulation, Λ/ρ, where ρ is the density of the material in which the cosmogenic neutron flux generates ^3He_c. In soils with a density of 1.1 g/cm^3 – our field-measured soil density in the Hanalei basin – the characteristic thickness of the ^3He_c accumulation zone is 1.45 m. Measured ^3He_c concentrations in such a field setting thus mainly reflect mass loss rates in the upper few meters below the Earth's surface, and are insensitive to mass losses that may be occurring at greater depth, such as those occurring by chemical erosion in deep weathering profiles (e.g., Dixon et al., 2009; Ferrier et al., 2010). Consequently, ^{3}He-based erosion rates should be compared to the sum of the physical and chemical erosion fluxes that occur in the upper few meters below the hillslope surface.

We are unaware of field constraints on the depths of chemical weathering fluxes in the Hanalei basin, and therefore cannot say definitively how much of the chemical weathering fluxes in the Hanalei basin are generated within the upper few meters below the hillslope surface. Mass fluxes inferred from ^{3}He concentrations in olivine are thus open to a range of interpretations between two end-member scenarios. In one end-member scenario, all the chemical erosion in the basin happens within a few meters of the hillslope surface (i.e., the zone in which cosmogenic ^{3}He accumulates). In this case, measured ^{3}He concentrations should be interpreted as reflecting the sum of physical and chemical erosion rates, and ^{3}He-based erosion rates should be compared to modern total mass fluxes. Under this interpretation, modern total erosion rates in the Hanalei basin (545 ± 128 t km^{-2} yr^{-1}) would be $<2.3 \pm 0.5$ times faster than the ^{3}He-based erosion rates (>238 t km^{-2} yr^{-1}). In the second end-member scenario, chemical erosion happens only at depth, below the ^{3}He accumulation zone. In this case, ^{3}He concentrations should be

interpreted as reflecting physical erosion rates but not chemical erosion rates, and ^{3}He-based erosion rates should be compared to modern physical erosion rates (406 ± 116 t km^{-2} yr^{-1}), which are <1.7 ± 0.5 times faster than the ^{3}He-based erosion rate. Between these two end-member scenarios lie a range of intermediate scenarios in which a portion of the chemical weathering flux happens within the ^{3}He accumulation zone and a portion happens below it. We therefore interpret modern erosional fluxes within the ^{3}He accumulation zone to be between <2.3 ± 0.6 and <1.7 ± 0.5 times faster than average mass fluxes in this zone over the past several thousand years in the Hanalei basin. That is, these data suggest that modern erosion rates in the Hanalei basin are elevated above millennial-scale erosion rates by approximately a factor of two, but they do not rule out the possibility that modern and millennial-scale erosion rates are the same.

In sum, the collection of erosion rates imply that modern erosion rates in the Hanalei basin are <1.7 ± 0.5 to 3.1 ± 0.8 times faster than erosion rates averaged over the past several thousand to several million years (Figure 6; Table 5). These long-term erosion rate estimates provide a baseline for management of the Hanalei basin. Both kyr-scale and Myr-scale erosion rates are substantially higher than recommended sediment fluxes implied by total maximum daily loads (TMDL) for total suspended solids in the Hanalei River (Hawaii Department of Health, 2008). Target TMDL limits for total suspended solid fluxes in the Hanalei estuary are as low as 1.58 t/day during dry season baseflow and as high as 3.24 t/day for wet season storms at the 2% not-to-exceed level, which, given the Hanalei basin's drainage area of 60.04 km^{2}, correspond to annual suspended sediment fluxes of 9.7-19.7 t km^{-2} yr^{-1} (Hawaii Department of Health, 2008). If suspended sediment fluxes constitute roughly two-thirds of the Hanalei basin's long-

term mass flux, as we estimate they do at present (369 t km^{-2} yr^{-1}/545 t km^{-2} yr^{-1} = 68%), then the TMDL recommendations imply total annual mass fluxes of 14.4-29.3 t km^{-2} yr^{-1}. Hence, the TMDL-recommended levels for total suspended solid fluxes in the Hanalei River are at least 8-17 times lower than kyr-scale average suspended sediment fluxes implied by our ^{3}He measurements. Given the high natural sediment flux background, meeting the TMDL recommended levels for the Hanalei River may be a significant challenge. We stress that this result applies only to the Hanalei River and not to other rivers on Kaua‘i, since the absence of modern fluvial sediment flux measurements in other basins prevents the direct comparison of long-term and short-term erosion rates in all basins on Kaua‘i except the Hanalei.

Alternative interpretations of ^{3}He data under hypothetical scenarios

The estimates of E_{3Hec} in Table 2 were calculated under the assumption that the sampled olivines were derived from sources that were uniformly distributed throughout the basins. We do not have field observations that would justify alternative interpretations, as olivine sands are abundant throughout the Hanalei basin, and shield stage flows from Kaua‘i are generally olivine rich (Mukhopadhyay et al., 2003; Gayer et al., 2008). Nonetheless, we can consider a few hypothetical scenarios in which olivines are not uniformly distributed within the sampled basins, to show that estimates of E_{3Hec} in such scenarios are not likely to differ greatly from those in Table 2. Consider, for example, the 1.73 km^2 basin above sample HAN003, in which the uppermost 0.31 km^2 of the basin stands atop the high-altitude, low-gradient Wai‘ale‘ale plateau. Because the plateau has a much shallower gradient than the rest of the HAN003 basin, it is

conceivable that the part of the basin atop the plateau might have contributed relatively little olivine to the sampled stream sediment. If we consider an extreme scenario in which none of the sampled olivines were derived from the plateau, then a different estimate of E_{3Hec} can be calculated with Equation 2 by using the mean value of P_{3Hec} in the part of the basin that lies below the plateau (i.e., P_{3Hec} = 146 at g^{-1} yr^{-1}). Because this value of P_{3Hec} is 90% as high as the mean P_{3Hec} in the entire basin, the revised estimate of minimum E_{3Hec} would be 90% as fast as that reported in Table 2. If we apply the same hypothetical scenario to the samples HAN006 and HAN020A, in which high-altitude plateaus comprise 2.4% and 0.9% of the basin areas, respectively, we calculate estimates of E_{3Hec} that are 1.5% and 1.2% slower, respectively, than the reported estimates in Table 2. The sample HAN011 would require no similar reinterpretation because no low-gradient plateaus exist within that basin.

One can consider a similar hypothetical scenario for the main stem sample HAN017. Because the topography in the western side of the Hanalei basin is considerably steeper than that on the eastern side, it is conceivable that erosion rates might be higher on the western side of the basin, and that more olivines might be contributed to the channel network from the western side of the basin. If we consider an extreme scenario in which all the sampled olivines at HAN017 were derived from the western side of the Hanalei basin, then the appropriate value of P_{3Hec} to apply in Equation 2 would be the mean value of P_{3Hec} in the western side of the basin. The mean value of P_{3Hec} in the western side of the basin is 3% higher than the mean value of P_{3Hec} throughout the entire basin, and consequently the estimate of E_{3Hec} would be 3% higher than that reported in Table 2 (i.e., >245 ± 59 t km^{-2} yr^{-1}). Since, in this scenario,

millennial-scale erosion rates on the eastern side of the basin (which composes 40% of the basin area) would be unconstrained by the ^{3}He measurements, this would permit the possibility that millennial-scale erosion rates might be as high as modern mass fluxes in the Hanalei basin (545 ± 128 t km^{-2} yr^{-1}). For this to be the case, however, millennial-scale erosion rates in the eastern side of the basin would have to average 1000 t km^{-2} yr^{-1}, over four times as fast as erosion rates in the western side of the basin. We consider this unlikely, given that average hillslope gradients in the eastern side of the basin are shallower than those on the western side. Thus, even in extreme scenarios in which no olivines were contributed to the channel network from either the high-altitude plateaus or the east side of the Hanalei basin, the resulting estimates of $E_{3\mathrm{Hec}}$ would differ from those in Table 2 by no more than 10%.

A second set of hypothetical scenarios concerns the depths from which olivines were eroded from the hillslope. As noted in the Methods section, we observed abundant olivine grains in stream sediment at each of the sample sites. This contrasts with observations of olivine-poor soils elsewhere on Kaua‘i and other Hawaiian islands, which suggest that olivines weather to completion in many Hawaiian soils, at least in lower-gradient soils with longer residence times than those that dominate the Hanalei basin (e.g., Vitousek et al., 1997; Chadwick et al., 1999; 2003). The absence of olivines in other Hawaiian soils and the presence of landslide scars throughout the study basins raise the possibility that the olivines in Hanalei stream sediment may not be derived from hillslope soils, but instead may be derived from less weathered material excavated at depth (e.g., by landslides or rockfall). If this were the case, olivines would experience a shorter cosmogenic exposure history than is implicitly assumed by Equation 2, which is

derived from an assumption that the sampled olivines were exhumed steadily from depth all the way to the hillslope surface (Lal, 1991). That is, if the sampled olivines had been sourced only from the base of landslide scars, erosion rates calculated with Equation 2 would overestimate the true erosion rates.

We cannot evaluate the likelihood of this scenario directly, because we do not have field measurements of soil olivine abundances throughout the study basins. We can, however, consider an extreme scenario in which all the olivines in stream channels are derived from material at the base of landslide scars, and evaluate how this would affect estimates of erosion rates calculated with Equation 2. That is, we can consider a scenario in which the sampled olivines are excavated from the base of landslide scars of thickness H, and are deposited in the channel network without further exposure to cosmogenic radiation. The hillslopes in this scenario erode steadily before landsliding; that is, we do not consider temporal fluctuations in erosion rates that would cause ^{3}He concentrations to fluctuate about a long-term mean (e.g., Bierman and Steig, 1996; Ferrier and Kirchner, 2008). In this scenario, Equation 2 can be used to estimate pre-landslide erosion rates if $P_{3\mathrm{Hec}}$ is taken to be the production rate of $^3\mathrm{He_c}$ at the base of the landslide scar, rather than at the hillslope surface (e.g., Heimsath et al., 1997). At the base of a landslide scar, $P_{3\mathrm{Hec}}$ is lower than that at the hillslope surface by a factor of $\exp(-\rho_s H/\Lambda)$, where ρ_s is the soil density and Λ is the attenuation length scale of cosmogenic neutrons (e.g., Gosse and Phillips, 2001). For H = 44 cm (the mean thickness of 20 landslide scars examined by Scott (1969) in Oahu's Koolau Range) and ρ_s = 1.1 g/cm^3 (our field-measured soil density in the Hanalei basin), $P_{3\mathrm{Hec}}$ at the base of the landslide scars would be 74% as fast as that at the surface. Erosion rates prior to landsliding in this extreme scenario would

therefore be 26% slower than the estimated erosion rates in Table 2. Considering that Myr-scale estimates of erosion rates vary by a factor of 40 across Kaua‘i (Figure 2), we suggest that the differences between estimated and actual erosion rates in this scenario would be relatively small.

Lastly, we consider a hypothetical scenario for sample HAN003, whose ^{3}He-based erosion rate of >390 ± 43 t km^{-2} yr^{-1} is 1.6-3.1 times faster than those in the other four sample basins. This is a relatively small spatial variation in erosion rates; differences of at least this size are common among basin-averaged erosion rates in similar studies (e.g., Granger et al., 1996; Kirchner et al., 2001; Hewawasam et al., 2003; Ferrier et al., 2005; Norton et al., 2010; DiBiase and Whipple, 2011). However, we acknowledge that it is theoretically possible that ^{3}He concentrations in olivines in the HAN003 basin might be influenced by a deep-seated landslide that can be seen in the topography high in the basin. If this deep-seated landslide were currently creeping downslope, it might be contributing olivines with low ^{3}He concentrations from depth directly to the channel, which would cause the estimated erosion rate to be higher than the true basin-averaged erosion rate. We are unaware of evidence that would suggest that this is actually occurring, as the absence of disturbed vegetation on the deep-seated landslide in the satellite images suggests it is not a very recent failure. We note, however, that because the measured ^{3}He concentration in each sample is an average over many olivine grains (Table 2), the extent to which such a process could bias the estimated erosion rate would depend on the fraction of the sampled olivines that were sourced from the deep-seated landslide (e.g., Brown et al., 1995; Bierman and Steig, 1996). Future

field measurements will be required to determine if the landslide is in fact creeping down slope and whether it is a major source of ^{3}He-poor olivines.

Table 5: Erosion rates in the Hanalei basin, Kaua‘i.

Method	Rate ($t\ km^{-2}\ yr^{-1}$)	Timescale	Comments
Volumetric excavation	175 – 309 (range)	1.5-4.43 Myr	Range in rates from minimum and maximum estimates of initial topography
^{3}He in detrital olivines	126 – 390 (minima)	4-13 kyr (maxima)	Range in rates over the five sampled catchments; each is a minimum estimate
Fluvial and subsurface fluxes (2003-2009)	545 ± 128 (mean ± s.e.)	5 years	Suspended sediment (USGS) + bedload (assumed) + fluvial solutes (Dessert et al., 2003) + groundwater solutes (Li, 1988)
Landslide scars (2004-2010)	30 – 47 (range)	5.99 years	Assumes 100% delivery of landslide material to streams

Erosion by shallow landsliding in the Hanalei basin

Comparing the landslide inventories in the QuickBird and WorldView-2 images revealed 62 new scars in the 2010 image that were not visible in the 2004 image, 36 of which we classified as “most certain”, and 26 of which we classified as “less certain”. We calculated minimum bounds on landslide-derived physical erosion rates with Equation 6 from the subset of 36 “most certain” scars, and calculated maximum bounds on landslide-derived physical erosion rates from the entire set of 62 new scars. Given an area of 48.21 km^2 that was jointly mappable in both satellite images, the 5.99-year time interval between the QuickBird and WorldView-2 images, and our field-measured soil density of 1.1 g/cm^3, the number of new landslide scars in the WorldView-2 image relative to the QuickBird image implies a landslide-derived physical erosion rate of E_L = 30-47 $t\ km^{-2}\ yr^{-1}$ over the entire Hanalei basin. If we approximate the flux of

landslide-derived material to be a source of physical sediment but a negligible source of solutes, a landslide-derived erosion rate of 38.5 ± 8.5 t km^{-2} yr^{-1} represents 10 ± 4% of the basin's physical sediment flux that was measured at the USGS monitoring station over roughly the same interval (406 ± 116 t km^{-2} yr^{-1}).

Implicit in the above calculation of E_L is an assumption that the area of each mapped scar is the area from which material was excavated, and does not include areas where landslide-derived material was deposited. Such an assumption may not be warranted in all cases, as observations of landslide scars in the Hanalei basin during low-altitude helicopter flights suggest that material may be deposited at the toes of some landslide scars (Stock and Tribble, 2010). In Figures 4A and 4B, for example, roughly 5% of the area of the two longest scars appears to be blanketed by deposits at their toes, while approximately 40% of the area of the smaller scar in Figure 4A appears to be covered by deposits at its toe. We do not have measurements of deposit size in all the landslide scars in the Hanalei basin, but our photographs of scars from helicopter surveys suggest that deposits cover <10% of the total scar area in most scars. In our mapping of landslide scars we did not attempt to estimate the fraction of each scar's area that was covered by deposit, because it was not possible to distinguish between source area and deposit at the resolution of the satellite images (Figure 5). Instead, we note that a fraction of the area of each mapped scar may consist of deposit, and stress that the estimate of E_L should be considered an upper bound on the rate at which landslides mobilize hillslope material.

Also implicit in the calculation of E_L is an assumption that all material excavated from landslide scars was transferred to the stream network. Field observations suggest,

however, that some material mobilized by landslides may be stored on hillslopes before being delivered to the stream network, such as the material deposited at the base of the smaller scar in Figure 4A. It is difficult to estimate in the satellite images what fraction of the material excavated by landslides directly enters the channel network; the resolution of the satellite images and partial revegetation of the scars prevent determining that definitively. Comparisons of scar locations with the location of the channel network suggest that as many as 50-85% of the new landslide scars in the WorldView-2 satellite image may not be directly connected to the channel network. The connectivity between landslide scars and the channel network could be quantified more precisely if the landslide scars could be accessed in the field shortly after their occurrences, but this rough estimate nonetheless suggests that a considerable fraction of landslide-mobilized material may be stored on hillslopes before entering the channel network.

Because these two assumptions provide upper limits on the erosion of landslide-derived material, we consider our estimate of E_L to be an upper bound on the flux of landslide-derived material to the channel network during 2004-2010. Determining what fraction of landslide-derived material is delivered to the channel network will require extensive field mapping of landslide scars and deposits, work that is beyond the scope of this study. We therefore consider 30-47 t km^{-2} yr^{-1} to be an upper bound on landslide-derived erosion rates in the Hanalei basin during 2004-2010. We emphasize that this estimate pertains only to landslide material discharging directly into the channel network; it does not account for erosion of landslide scars by gullying or remobilization of older landslide deposits.

This estimate of landslide-derived erosion rates is toward the low end of landslide-derived erosion rates found elsewhere in the Hawaiian Islands. Wentworth (1943), for instance, estimated that shallow landsliding was responsible for soil erosion at a rate of 0.79 mm/yr over eight years of observation over a 39 km^2 region in Oahu's Koolau Range. Multiplying this by a soil density of 1.1 g/cm^3 (our field measurement of soil density in the Hanalei basin) yields a physical erosion rate of 869 t km^{-2} yr^{-1}. In a similar study in a 7 km^2 region in the Koolau Range, Scott (1969) used an estimated scar revegetation time of 3-4 years and the measured or estimated volumes of 132 soil-based landslide scars to calculate that shallow landsliding was responsible for 0.38-0.87 mm/yr of soil erosion in this field area. If we again assume a soil density of 1.1 g/cm^3, this corresponds to physical erosion rates of 418-957 t km^{-2} yr^{-1}. Two decades later, Peterson et al. (1993) and Ellen et al. (1993) used a series of 19 aerial photographs taken between 1940 and 1989 to map 1790 landslide scars in the 220 km^2 Honolulu district of the Koolau Range. Multiplying their calculated eroded volume by an assumed soil density of 1.1 g/cm^3 and dividing by the surveyed area and the 49-year time span yields a physical erosion rate of 22 t km^{-2} yr^{-1}. These estimates of E_L were measured over different time intervals and spatial scales, and thus differences among these estimates may reflect temporal variations in landslide occurrence, differences in the likelihood of observing large events over different observation periods, or differences in the study areas themselves.

As in any study that calculates landslide volumes from landslide areas, this estimate of landslide-derived erosion rates is dependent upon the accuracy of the applied landslide area-volume scaling relationship in the study area (e.g., Korup et al., 2012). As

noted in the Methods section, we applied an area-volume scaling relationship based on a global inventory of 2136 soil-based landslide scars (Larsen et al., 2010). We were unable to verify the accuracy of this landslide area-volume scaling relationship in the Hanalei basin, because the Hanalei basin's steep terrain and dense vegetation prevented access to landslide scars in the field and therefore prevented direct measurement of landslide scar volumes. However, the predicted erosion rates can be compared to erosion rates predicted by a different scaling relationship based on the areas and volumes of 20 landslide scars that Scott (1969) was able to access and measure directly in similar terrain on Oahu. Because the scars examined by Scott (1969) had depths that were largely insensitive to scar area, the scaling relationship of Scott (1969) predicts a weaker dependence of landslide volume on area ($V = 0.359A_L^{1.040}$) than does the scaling relationship of Larsen et al. (2010). Our field observations of landslide scars from helicopter surveys are similarly consistent with little variation in landslide thickness with scar area. Applying the area-volume scaling relationship from Scott's measurements yields landslide-derived erosion rates of 15-19 t km^{-2} yr^{-1}, which is 1.5-3 times smaller than the erosion rates of 30-47 t km^{-2} yr^{-1} estimated from the scaling relationship of Larsen et al. (2010). Here we have chosen to apply the scaling relationship of Larsen et al. (2010) because it is based on a much larger dataset than that in Scott (1969). We caution that the applicability of this scaling relationship in the Hanalei basin remains to be validated, and that other area-volume relationships could accommodate landslide-derived erosion rates that differ from our estimate by over a factor of two. It is unlikely, however, that using a different area-volume scaling relationship could yield a landslide-

derived erosion rate that would account for the entire fluvial sediment flux measured between 2003 and 2009.

Thus, even considering the uncertainties in estimating E_L, our calculations imply that landslide-derived material was a small fraction of the Hanalei River's fluvial sediment flux between 2003 and 2009. This is consistent with previously published observations suggesting that landslides may not have been the primary source of suspended sediment in the Hanalei River over this time interval. For instance, measurements of stream discharge and suspended sediment concentrations in the Hanalei River during this period are consistent with a dominantly streambank source of suspended sediment. Stock and Tribble (2010) reported that hystereses between stream discharge and suspended sediment concentrations in the Hanalei River tend to be weak – that is, that temporal lags between stream discharge and suspended sediment concentrations tend to be short. This observation is consistent with rapid mobilization of sediment from sources that are sensitive to river stage (e.g., legacy sediment in streambanks), but inconsistent with mobilization of sediments that take longer to enter the channel network (e.g., soils higher in the basin). This is also consistent with measurements of ^{137}Cs in stream sediment, streambank sediment, and hillslope soil profiles in the Hanalei basin, which led Ritchie and Pedone (2008) to suggest that the dominant source of suspended sediment was most likely streambank sediment or hillslope soils at depth, but was unlikely to be soils at the hillslope surface. Thus, observations in both Stock and Tribble (2010) and Ritchie and Pedone (2008) are consistent with the possibility that streambank erosion may be the dominant source of suspended sediment in the Hanalei River. This possibility cannot be addressed directly in

the present study because we do not have measurements of streambank erosion rates, but it is consistent with the small size of our estimate of E_L relative to the suspended sediment flux.

CONCLUSIONS AND IMPLICATIONS

The measurements presented here lead to several conclusions about erosional patterns on Kaua'i in space and time. First, basin-averaged erosion rates across Kaua'i over the past several million years are highly variable in space, ranging from 8 to 335 t km^{-2} yr^{-1}. Both erosion rates and the extent of basin excavation over this timescale are positively correlated with modern mean annual precipitation. To the extent that modern spatial patterns in precipitation rates are representative of precipitation patterns over the past 4-5 Myr, these data are consistent with the notion that rainfall rates positively influence long-term erosion rates on volcanic islands. Although correlations between precipitation rates and long-term erosion rates or exhumation rates have been observed in the Atacama desert (Owen et al., 2010) and the Washington Cascades (Reiners et al., 2003; Moon et al., 2011), such correlations are more frequently not apparent in compilations of erosion rate and climate measurements (e.g., Walling and Webb, 1983; Riebe et al., 2001; von Blanckenburg, 2005; Portenga and Bierman, 2011). We suggest that the observed correlation between precipitation rates and erosion rates on Kaua'i may be apparent because spatial variations in precipitation rates are so large and because variations in potentially confounding factors like lithology and rock uplift rates are relatively small. This suggests that mean annual precipitation may play an important role in setting the efficiency of erosional processes like bedrock river incision and hillslope

soil transport on volcanic islands, which would provide support for proposed feedbacks among climate, erosion, and the structure of mountain belts (e.g., Willett, 1999; Beaumont et al., 2001; Whipple and Meade, 2004; Stolar et al., 2007; Roe et al., 2008; Whipple, 2009). These feedbacks propose that spatially focused precipitation drives spatially focused erosion and thereby modulates a mountain belt's width and height, which themselves modulate spatial patterns in precipitation. These proposed feedbacks hinge on the requirement that bedrock erosion is more efficient where precipitation rates are higher. This is a prediction we will address in future studies.

Second, in the Hanalei basin, modern erosion rates are 1.4-3.1 times faster than erosion rates averaged over the past several million years and over the past several thousand years, a difference that we suggest is relatively small, given that Myr-scale erosion rates vary across Kaua'i by more than a factor of 40. Whether the temporal variations in erosion rates in the Hanalei basin are representative of other basins on Kaua'i cannot be addressed with these data, but we plan to address this in future studies. Measured ^{3}He concentrations in detrital olivine imply that erosion rates over the past several thousand years are at least 8-17 times higher than regulatory targets for modern Hanalei River sediment fluxes (EPA, 2008; Hawaii Dept. of Health, 2008). Because Hanalei River fluvial sediment fluxes were only monitored from 2003 to 2009, and because our ^{3}He-based erosion rate estimates are averaged over the past several thousand years, the measurements compiled in this paper cannot directly show whether increases in human development in the Hanalei basin over the past century have led to increases in erosion rates. However, upstream of the USGS Hanalei River gauging station, the absence of infrastructure suggests that human modification of the upper 80% of the basin

has been relatively minor over the past century. This in turn suggests that any changes in sediment delivery upstream of the USGS gauge over the past century are unlikely to be a direct result of changes in land use. Changes in vegetation over the past century may have affected rates of soil delivery to channels, but our data compilation here cannot resolve that, and this remains a question for future work.

Third, shallow landsliding accounted for 10 ± 3% of the physical sediment flux in the Hanalei River between 2004 and 2010, implying that other erosional processes such as soil creep, streambank erosion, and overland flow (potentially including post-failure erosion of landslide scars) were likely responsible for the bulk of the delivery of hillslope material to the channel network during the monitoring period.

The broad similarity between erosion rates in the Hanalei basin over annual, millennial, and million-year time scales gives the impression that erosion has been relatively steady over millions of years. This contrasts with the knowledge that Kaua‘i’s topography must have been transiently evolving over the past ~4 Myr, since all shield volcanoes build initially smooth domes that subside and grow more dissected over time. Indeed, the dramatic changes in hydrology that an island experiences over its lifetime might lead one to expect even more dramatic differences in island erosion rates over time. Our measurements show that similarity among basin-averaged erosion rates over different time scales is not necessarily a signature of steady-state topography. Instead, they show that even in transient landscapes, basin-averaged erosion rates measured over different time scales may give the impression that erosion has been steady over a wide range of time scales.

Overall, the erosion rates presented here suggest an empirical link between erosion rates and precipitation rates, and they provide a first step toward a more comprehensive quantitative basis for conservation and management of Hawaiian reefs and watersheds. They also provoke a number of further questions about volcanic ocean island evolution. For instance, what are the general conditions that control how erosion rates evolve in time and space over the lifespan of an island? Are modern erosion rates across Kaua‘i a strong function of rainfall rates, as the correlation between Myr-scale erosion rates and mean annual precipitation suggests they should be? Lastly, why are erosion rates so slow in a landscape that is so steep and so wet? Kaua‘i has many basins with mean hillslope gradients steeper than 100% and mean annual precipitation rates that are among the highest on Earth, yet erosion rates on Kaua‘i are not high on the global scale. In the Hanalei basin, for instance, our mean erosion rate estimates range from 126 to 545 t km^{-2} yr^{-1} – comparable to the global average erosion rate of 140 t km^{-2} yr^{-1} (Wilkinson and McElroy, 2007; Gayer et al., 2008) – while estimates of erosion rates on other volcanic islands are as high as >10,000 t km^{-2} yr^{-1} (Louvat et al., 2008). This suggests that there is still much that is not understood about climatic and topographic controls on erosion rates.

Our observations suggest that determining what sets the pace of landscape evolution on volcanic ocean islands over time and space is an open challenge. Given the suitability of volcanic islands as natural experiments in landscape evolution, we suggest that addressing that challenge may provide insights into the general evolution of topography, both on islands and on continents. This will require advances in theoretical

models of volcanic island evolution as well as tests of those models against measurements of erosion rates, such as those presented here.

ACKNOWLEDGMENTS

We thank Herdis Schopka, associate editor Anne Jefferson, editor Hope Jahren, and one anonymous reviewer for their suggestions that substantially improved the manuscript. We thank Stéphane Escrig and Zhongxing Chen for the Li, Sm, U, and Th measurements on the olivine aliquots and Ken Farley for replicating the helium analyses on powdered olivine samples. We thank Mike Lamb, Ben Mackey, Joel Scheingross, and Chuck Blay for enlightening discussions and assistance with field sampling. We also thank the US Fish and Wildlife Service for access through the Hanalei National Wildlife Refuge, and the Alapai and Napolis ohana for allowing access to the Hanalei River Trail. SM's field work was supported by the Earth & Planetary Science Department at Harvard University.

REFERENCES CITED

Andrews, J.N., and Kay, R.L.F., 1982, Natural production of tritium in permeable rocks: Nature, v. 298, p. 361-363.

Balco, G., Stone, J.O., Lifton, N.A., and Dunai, T.J., 2008, A complete and easily accessible means of calculating surface exposure ages or erosion rates from ^{10}Be and ^{26}Al measurements: Quaternary Geochronology, v. 3, p. 174-195.

Beaumont C., Jamieson, R.A., Nguyen, M.H., Lee, B., 2001, Himalayan tectonics explained by extrusion of a low-viscosity crustal channel coupled to focused surface denudation: Nature, v. 414, p. 738-742.

Bierman, P., and Steig, E.J., 1996, Estimating rates of denudation using cosmogenic isotope abundances in sediment: Earth Surface Processes and Landforms, v. 21, p. 125-139.

Brown, E.T., Stallard, R.F., Larsen, M.C., Raisbeck, G.M., and Yiou, F., 1995, Denudation rates determined from the accumulation of in situ produced ^{10}Be in the Luquillo experimental forest, Puerto Rico: Earth and Planetary Science Letters, v. 129, p. 193-202.

Calhoun, R.S., and Fletcher, C.H., 1999, Measured and predicted sediment yield from a subtropical, heavy rainfall, steep-sided river basin: Hanalei, Kauai, Hawaiian Islands: Geomorphology, v. 30, p. 213-226.

Chadwick, O.A., Derry, L.A., Vitousek, P.M., Huebert, B.J., and Hedin, L.O., 1999, Changing sources of nutrients during four millions years of ecosystem development: Nature, v. 397, p. 491-497.

Chadwick, O.A., Gavenda, R.T., Kelly, E.F., Ziegler, K., Olson, C.G., Elliott, W.C., and Hendricks, D.M., 2003, The impact of climate on the biogeochemical functioning of volcanic soils: Chemical Geology, v. 202, p. 195-23, doi:10.1016/j.chemgeo.2002.09.001.

Clague, D.A., 1996, The growth and subsidence of the Hawaiian-Emperor volcanic chain, *in* Keast, Allen, and Miller, S.E., eds., The origin and evolution of Pacific Island biotas, New Guinea to Eastern Polynesia: patterns and processes: Amsterdam, SPB Academic Publishing, p. 35-50.

Clague, D.A., and Dalrymple, G.B., 1988, Age and petrology of alkalic postshield and rejuvenated-stage lava from Kauai, Hawaii: Contributions to Mineralogy and Petrology, v. 99, p. 202-218.

Cox, E.F., and Ward S., 2002, Impact of elevated ammonium on reproduction in two Hawaiian scleractinian corals with different life history patterns: Marine Pollution Bulletin, v. 44, p. 1230-1235.

Craig, D.A., 2003, Geomorphology, development of running water habitats, and evolution of black flies on Polynesian Islands: BioScience, v. 53, p. 1079-1093.

Daly, C., Gibson, W.P., Taylor, G.H., Johnson, G.L., and Pasteris, P., 2002, A knowledge-based approach to the statistical mapping of climate: Climate Research, v. 22, p. 99-113.

Dana, J.D., 1890, Characteristics of Volcanoes: New York, Dodd, Mead, and Company, 399 p.

Dessert, C., Dupre, B., Gaillardet, J., Francois, L.M., and Allegre, C.J., 2003, Basalt weathering laws and the impact of basalt weathering on the global carbon cycle: Chemical Geology, v. 202, p. 257-273.

DiBiase, R.A., and Whipple, K.X., 2011, The influence of erosion thresholds and runoff variability on the relationships among topography, climate, and erosion rate: Journal of Geophysical Research, v. 116, F04036, doi: 10.1029/2011JF002095.

Dixon, J.L., Heimsath, A.M., and Amundson R., 2009, The critical role of climate and saprolite weathering in landscape evolution: Earth Surface Processes and Landforms, doi: 10.1002/esp.1836.

Draut, A.E., Bothner, M.H., Field, M.E., Reynolds, R.L., Cochran, S.A., Logan, J.B., Storlazzi, C.D., and Berg, C.J., 2009, Supply and dispersal of flood sediment from a steep, tropical watershed: Hanalei Bay, Kauai, Hawaii, USA: Geological Society of America Bulletin, v. 121, p. 574-585.

Ellen, S.D., Mark, R.K., Cannon, S.H., and Knifong, D.L., 1993, Map of debris-flow hazard in the Honolulu District of Oahu, Hawaii: US Geological Survey Open-File Report 93-213, 25 pp.

EPA, 2008, TMDL Report For Hanalei Bay Watershed: http://iaspub.epa.gov/tmdl_waters10/attains_impaired_waters.tmdl_report?p_tmdl_id=35294&p_tribe= (25 October 2011).

Fabricius, K.E., 2005, Effects of terrestrial runoff on the ecology of corals and coral reefs: review and synthesis: Marine Pollution Bulletin, v. 50, p. 125-146, doi: 10.1016/j.marpolbul.2004.11.028.

Farley, K.A., 2002, (U-Th)/He dating: Techniques, calibrations, and applications: Reviews in Mineralogy and Geochemistry, v. 47, p. 819-844, doi: 10.2138.rmg.2002.47.18.

Ferrier, K.L., Kirchner, J.W., and Finkel, R.C., 2005, Erosion rates over millennial and decadal timescales at Caspar Creek and Redwood Creek, Northern California Coast Ranges: Earth Surface Processes and Landforms, v. 30, p. 1025-1038, doi: 10.1002/esp.1260.

Ferrier, K.L., Kirchner, J.W., 2008, Effects of physical erosion on chemical denudation rates: A numerical modeling study of soil-mantled hillslopes: Earth and Planetary Science Letters, v. 272, p. 591-599, doi: 10.1016/j.epsl.2008.05.024.

Ferrier, K.L., Kirchner, J.W., Riebe, C.S., and Finkel, R.C., 2010, Mineral-specific chemical weathering rates over millennial timescales: Measurements at Rio Icacos, Puerto Rico: Chemical Geology, v. 277, p. 101-114, doi: 10.1016/j.chemgeo.2010.07.013.

Flinders, A.F., Ito, G., Garcia, M.O., 2010, Gravity anomalies of the Northern Hawaiian Islands: Implications on the shield evolutions of Kauai and Niihau: Journal of Geophysical Research, v. 115, B08412, doi: 10.1029/2009JB006877.

Gardner, T.A., Cote, I.M., Gill, J.A., Grant, A., and Watkinson, A.R., 2003, Long-term region-wide declines in Caribbean corals: Science, v. 301, p. 958-960.

Garcia, M.O., Swinnard, L., Weis, D., Greene, A.R., Tagami, T., Sano, H., and Gandy, C.E., 2010, Petrology, geochemistry and geochronology of Kaua‘i lavas over 4.5 Myr: Implications for the origin of rejuvenated volcanism and the evolution of the Hawaiian plume: Journal of Petrology, v. 51, p. 1507-1540.

Gavenda, R.T., 1992, Hawaiian Quaternary paleoenvironments: A review of geological, pedological, and botanical evidence: Pacific Science, v. 46, p. 295-307.

Gayer, E., Mukhopadhyay, S., and Meade, B.J., 2008, Spatial variability of erosion rates inferred from the frequency distribution of cosmogenic ^{3}He in olivines from Hawaiian river sediments: Earth and Planetary Science Letters, v. 266, p. 303-315.

Goehring, B.M., Kurz, M.D., Balco, G., Schaefer, J.M., Licciardi, J., and Lifton, N., 2010, A reevaluation of in situ cosmogenic ^{3}He production rates: Quaternary Geochronology, v. 5, p. 410-418.

Granger, D.E., Kirchner, J.W., and Finkel, R.C., 1996, Spatially averaged long-term erosion rates measured from in situ-produced cosmogenic nuclides in alluvial sediment: Journal of Geology, v. 104, p. 249-258.

Gosse, J.C., and Phillips F.M., 2001, Terrestrial in situ cosmogenic nuclides: theory and application: Quaternary Science Reviews, v. 20, p. 1475-1560.

Hack, J.T., 1960, Interpretation of erosional topography in humid temperate regions: American Journal of Science, v. 258-A, p. 80-97.

Hawaii Department of Health, 2008, Total maximum daily loads for the Hanalei Bay watershed, Phase 1 – Streams and estuaries. Environmental Health Administration, Environmental Planning Office, Honolulu, HI, 393 p: http://hawaii.gov/health/environmental/env-planning/pdf/hanalei_tmdl.pdf (25 October 2011).

Heimsath, A.M., Dietrich, W.E., Nishiizumi, K., and Finkel, R.C., 1997, The soil production function and landscape equilibrium: Nature, v. 388, p. 358-361.

Hewawasam, T., von Blanckenburg, F., Schaller, M., Kubik, P., 2003, Increase of human over natural erosion rates in tropical highlands constrained by cosmogenic nuclides: Geology, v. 31, p. 597-600.

Hildenbrand, A., Gillot, P.-Y., and Marlin, C., 2008, Geomorphological study of long-term erosion on a tropical volcanic ocean island: Tahiti-Nui (French Polynesia): Geomorphology, v. 93, p. 460-481.

Hill, B.R., Fuller, C.C., and DeCarlo, E.H., 1997, Hillslope soil erosion estimated from aerosol concentrations, North Halawa Valley, Oahu, Hawaii: Geomorphology, v. 20, p. 67-79.

Holcomb, R.T., Reiners, P.W., Nelson, B.K., and Sawyer, N.E., 1997, Evidence for two shield volcanoes exposed on the island of Kauai, Hawaii: Geology, v. 25, p. 811-814.

Hotchkiss, S., and Juvik, J.O., 1999, A late-Quaternary pollen record from Ka‘au Crater, O‘ahu, Hawai‘i: Quaternary Research, v. 52, p. 115-128.

Hotchkiss, S., Vitousek, P.M., Chadwick, O.A., and Price, J., 2000, Climate cycles, Geomorphological change, and the interpretation of soil and ecosystem development: Ecosystems, v. 3, p. 522-533.

Hovius, N., Stark, C.P., and Allen, P.A., 1997, Sediment flux from a mountain belt derived by landslide mapping: Geology, v. 25, p. 231-234.

Jefferson A., Grant, G.E., Lewis S.L., and Lancaster, S.T., Coevolution of hydrology and topography on a basalt landscape in the Oregon Cascade Range, USA: Earth Surface Processes and Landforms, doi: 10.1002/esp.1976.

Jones, B.L., Chinn, S.S.W., and Brice, J.C., 1984, Olokele rock avalanche, island of Kauai, Hawaii: Geology, v. 12, p. 209-211.

Kirchner, J.W., Finkel, R.C., Riebe, C.S., Granger, D.E., Clayton, J.L., King, J.G., and Megahan, W.F., 2001, Mountain erosion over 10 yr, 10 k.y., and 10 m.y. time scales: Geology, v. 29, p. 591-594.

Korup, O., Görüm, T., and Hayakawa, Y., 2012, Without power? Landslide inventories in the face of climate change: Earth Surface Processes and Landforms, v. 37, p. 92-99, doi: 10.1002/esp.2248.

Kurz, M.D., 1986, Cosmogenic helium in a terrestrial igneous rock: Nature, v. 320, p. 435-439.

Lal, D., 1989, An important source of ^{4}He (and ^{3}He) in diamonds: Earth and Planetary Science Letters, v. 96, p. 1-7.

Lal, D., 1991, Cosmic ray labeling of erosion surfaces: in situ nuclide production rates and erosion models: Earth and Planetary Science Letters, v. 104, p. 424-439.

Lamb M.P., Howard, A.D., Dietrich, W.E., and Perron, J.T., 2007, Formation of amphitheater-headed valleys by waterfall erosion after large-scale slumping on Hawai‘i: Geological Society of America Bulletin, v. 119, p. 805-822, doi: 10.1130/B25986.

Langbein, W.B., and Schumm, S.A., 1958, Yield of sediment in relation to mean annual precipitation: American Geophysical Union Transactions, v. 39, p. 1076-1084.

Larsen, I.J., Montgomery, D.R., and Korup, O., 2010, Landslide erosion controlled by hillslope material: Nature Geoscience, v. 3, p. 247-251.

Li, Y.-H., 1988, Denudation rates of the Hawaiian Islands by rivers and groundwaters: Pacific Science, v. 42, p. 253-266.

Lohse, K.A., and Dietrich, W.E., 2005, Contrasting effects of soil development on hydrological properties and flow paths: Water Resources Research, v. 41, W12419, doi: 10.1029/2004WR003403.

Louvat, P., and Allegre, C.J., 1997, Present denudation rates on the island of Réunion determined by river geochemistry: Basalt weathering and mass budget between chemical and mechanical erosions: Geochimica et Cosmochimica Acta, v. 61, p. 3645-3669.

Louvat, P., Gislason, S.R., and Allegre, C.J., 2008, Chemical and mechanical erosion rates in Iceland as deduced from river dissolved and solid material: American Journal of Science, v. 308, p. 679-726, doi: 10.2475/05.2008.02.

Macdonald, G.A., Davis, D.A., and Cox, D.C., 1960, Geology and ground-water resources of the Island of Kauai, Hawaii: Hawaii Division of Hydrography Bulletin 13.

Mark, R.K., and Moore, J.G., 1987, Slopes of the Hawaiian ridges: U.S. Geological Survey Professional Paper 1350, p. 101-107.

McDougall, I., 1979, Age of shield-building volcanism of Kauai and linear migration of volcanism in the Hawaiian Island chain: Earth and Planetary Science Letters, v. 46, p. 31-42.

Moberly, R., 1963, Rate of denudation in Hawaii: Journal of Geology, v. 71, p. 371-375.

Moon, S., Chamberlain, C.P., Blisniuk, K., Levine, N., Rood, D.H., and Hilley, G.E., 2011, Climatic control of denudation in the deglaciated landscape of the Washington Cascades: Nature Geoscience, v. 4, p. 469-473, doi: 10.1038/ngeo1159.

Moore, J.G., Clague, D.A., Holcomb, R.T., Lipman, P.W., Normark, W.R., and Torresan M.E., 1989, Prodigious submarine landslides on the Hawaiian Ridge: Journal of Geophysical Research, v. 94, p. 17465-17484.

Mukhopadhyay, S., Lassiter, J.C., Farley, K.A., and Bogue, S.W., 2003, Geochemistry of Kauai shield-stage lavas: Implications for the chemical evolution of the Hawaiian plume: Geochemistry Geophysics Geosystems, v. 4, 1009, doi: 10.1029/2002GC000342.

Niemi, N.A., Oskin, M., Burbank, D.W., Heimsath, A.M., and Gabet, E.J., 2005, Effects of bedrock landslides on cosmogenically determined erosion rates: Earth and Planetary Science Letters, v. 237, p. 480-498.

Norton, K.P., von Blanckenburg, F., and Kubik, P.W., 2010, Cosmogenic nuclide-derived rates of diffusive and episodic erosion in the glacially sculpted upper Rhone Valley, Swiss Alps: Earth Surface Processes and Landforms, v. 35, p. 651-662, doi: 10.1002/esp.1961.

Owen, J.J., Amundson, R., Dietrich, W.E., Nishiizumi, K., Sutter, B., and Chong, G., 2010, The sensitivity of hillslope bedrock erosion to precipitation: Earth Surface Processes and Landforms, v. 36, p. 117-135, doi: 10.1002/esp.2083.

Peterson, D.M., Ellen, S.D., and Knifong, D.L., 1993, Distribution of past debris flows and other rapid slope movements from natural hillslopes in the Honolulu District of Oahu, Hawaii: US Geological Survey Open-File Report 93-514.

Porter, S.C., 1979, Hawaiian glacial ages: Quaternary Research, v. 12, p. 161-187.

Porter, S.C., 1997, Late Pleistocene eolian sediments related to pyroclastic eruptions of Mauna Kea Volcano, Hawaii: Quaternary Research, v. 47, p. 261-276.

Portenga, E.W., and Bierman, P.R., 2011, Understanding Earth's eroding surface with ^{10}Be: GSA Today, v. 21, p. 4-10, doi: 10.1130/G111A.1.

Poveda, G., and Mesa, O.J., 2000, On the existence of Lloro (the rainiest locality on Earth): Enhanced ocean-land-atmosphere interaction by a low-level jet: Geophysical Research Letters, v. 27, p. 1675-1678.

PRISM Climate Group, Oregon State University, 2006: http://prism.oregonstate.edu (2010).

Rad, S.D., Allegre, C.J., and Louvat, P., 2007, Hidden erosion on volcanic islands: Earth and Planetary Science Letters, v. 262, p. 109-124.

Ramage, C.S., and Schroeder, T.A., 1999, Trade wind rainfall atop Mount Waialeale, Kauai: Monthly Weather Review, v. 127, p. 2217-2226.

Reiners, P.W., Nelson, B.K., and Izuka, S. K., 1998, Structural and petrologic evolution of the Lihue basin and eastern Kauai, Hawaii: GSA Bulletin, v. 111, p. 674-685.

Reiners, P.W., Ehlers, T.A., Mitchell, S.G., and Montgomery, D.R., 2003, Coupled spatial variations in precipitation and long-term erosion rates across the Washington Cascades: Nature, v. 426, p. 645-647.

Riebe, C.S., Kirchner, J.W., Granger, D.E., and Finkel, R.C., 2001, Minimal climatic control on erosion rates in the Sierra Nevada, California: Geology, v. 29, p. 447-450.

Ritchie, J.C., and Pedone, P., 2008, Determining sediment sources in the Hanalei River Watershed, Kaua'i, Hawaii: Proceedings of the 15th International Soil Conservation Organization, May 18-23, 2008, Budapest, Hungary.

Rogers, C.S., 1979, The effect of shading on coral reef structure and function: Journal of Experimental Marine Biology and Ecology, v. 41, p. 269-288.

Rogers, C.S., 1990, Responses of coral reefs and reef organisms to sedimentation: Marine Ecology Progress Series, v. 62, p. 185-202.

Roe, G. H., Whipple, K. X., and Fletcher, J. K., 2008, Feedbacks among climate, erosion, and tectonics in a critical wedge orogen: American Journal of Science, v. 308, p. 815-842, doi:10.2475/07.2008.01.

Schopka, H.H., and Derry, L.A., 2012, Chemical weathering fluxes from volcanic islands and the importance of groundwater: The Hawaiian example: Earth and Planetary Science Letters, v. 339-340, p. 67-78.

Scott, G.A.J., 1969, Relationships between vegetation and soil avalanching in the high rainfall areas of Oahu, Hawaii [Master's thesis]: Honolulu, University of Hawaii, Honolulu, 98 p.

Scott, G.A.J., and Street, J.M., 1976, The role of chemical weathering in the formation of Hawaiian amphitheatre-headed valleys: Zeitschrift für Geomorphologie, v. 20, p. 171-189.

Seidl, M.A., Dietrich, W.E., and Kirchner, J.W., 1994, Longitudinal profile development into bedrock: an analysis of Hawaiian channels: Journal of Geology, v. 102, p. 457-474.

Sherrod, D.R., Sinton, J.M., Watkins, S.E., and Brunt, K.M., 2007, Geologic map of the state of Hawai‘i: U.S. Geological Survey Open-File Report 2007-1089.

Stearns, H.T., 1940, Geology and ground-water resources of the islands of Lanai and Kahoolawe, Hawaii: Hawaii Division of Hydrography Bulletin 6.

Stearns, H.T., and Macdonald, G.A., 1942, Geology and ground-water resources of the island of Maui, Hawaii: Hawaii Division of Hydrography Bulletin 7.

Stearns, H.T., and Macdonald, G.A., 1947, Geology and ground-water resources of the island of Molokai, Hawaii: Hawaii Division of Hydrography Bulletin 11.

Stock, J.D., and Montgomery, D.R., 1999, Geologic constraints on bedrock river incision using the stream power law: Journal of Geophysical Research, v. 104, p. 4983-4993.

Stock, J.D., and Tribble, G., 2010, Erosion and sediment loads from two Hawaiian watersheds, *in* Proceedings, Second Joint Federal Interagency Conference, Las Vegas, NV, 11 pp.

Stolar, D., Roe, G., and Willett, S., 2007, Controls on the patterns of topography and erosion rate in a critical orogen: Journal of Geophysical Research, v. 112, F04002, doi: 10.1029/2006JF000713.

Takesue, R.K., Bothner, M.H., and Reynolds R.L., 2009, Sources of land-derived runoff to a coral reef-fringed embayment indentified using geochemical tracers in nearshore sediment traps: Estuarine, Coastal and Shelf Science, v. 85, p. 459-471.

Telesnicki, G.J., and Goldberg, W.M., 1995, Effects of turbidity on the photosynthesis and respiration of two south Florida reef coral species: Bulletin of Marine Science, v. 57, p. 527-539.

Tucker, G.E., 2009, Natural experiments in landscape evolution: Earth Surface Processes and Landforms, v. 34, p. 1450-1460, doi: 10.1002/esp.1833.

Tucker, G.E., and Whipple, K.X., 2002, Topographic outcomes predicted by stream erosion models: Sensitivity analysis and intermodal comparison: Journal of Geophysical Research, v. 107, doi: 10.1029/2001JB000162.

Turowski, J.M., Rickenmann, D., and Dadson, S.J., 2010, The partitioning of the total sediment load of a river into suspended load and bedload: a review of empirical data: Sedimentology, v. 57, p. 1126-1146, doi: 10.1111/j.1365-3091.2009.01140.x.

USGS National Water Information System, Hanalei River monitoring summary: http://waterdata.usgs.gov/nwis/nwisman/?site_no=16103000&agency_cd=USGS (17 June 2011).

Vitousek, P.M., Chadwick, O.A., Crews, T.E., Fownes, J.H., Hendricks, D.M., and Herbert, D., 1997, Soil and ecosystem development across the Hawaiian Islands: GSA Today, v. 7, p. 1-8.

von Blanckenburg, F., 2005, The control mechanisms of erosion and weathering at basin scale from cosmogenic nuclides in river sediment: Earth and Planetary Science Letters, v. 237, p. 462-479, doi: 10.1016/j.epsl.2005.06.030.

Walling, D.E., and Webb, B.W., 1983, Patterns of sediment yields, *in* Gregory, K.J., ed., Background to paleohydrology: London, John Wiley & Sons, Ltd., p. 69-100.

Wentworth, C.K., 1926, Pyroclastic geology of Oahu: Bernice P. Bishop Museum Bulletin, v. 30.

Wentworth, C.K., 1927, Estimates of marine and fluvial erosion in Hawaii: Journal of Geology, v. 35, p. 117-133.

Wentworth, C.K., 1943, Soil avalanches on Oahu, Hawaii: GSA Bulletin, v. 54, p. 53-64.

Western Regional Climate Center: http://www.wrcc.dri.edu/cgi-bin/cliMAIN.pl?hi9253; http://www.wrcc.dri.edu/cgi-bin/cliMAIN.pl?hi6565 (24 October 2011).

Whipple, K.X., 2009, The influence of climate on the tectonic evolution of mountain belts: Nature Geoscience, v. 2, p. 97-104, doi: 10.1038/ngeo413.

Whipple, K. X., and Meade, B. J., 2004, Controls on the strength of coupling among climate, erosion, and deformation in two-sided, frictional orogenic wedges at steady state: Journal of Geophysical Research, v. 109, doi:10.1029/2003jf000019.

White, S.E., 1949, Processes of erosion on steep slopes of Oahu, Hawaii: American Journal of Science, v. 247, p. 168-186.

Wilkinson, C., 2002, ed., Status of Coral Reefs of the World, Australian Institute of Marine Science, Townsville, Australia.

Wilkinson, B.H., and McElroy B.J., 2007, The impact of humans on continental erosion and sedimentation: Geological Society of America Bulletin, v. 119, p. 140-156, doi: 10.1130/B25899.

Willett, S.D., Orogeny and orography: The effects of erosion on the structure of mountain belts: Journal of Geophysical Research, v. 104, p. 28957-28981.

Winchell, H., 1947, Honolulu Series, Oahu, Hawaii: Geological Society of America Bulletin, v. 58, p. 1-48.

Yentsch, C.S., Yentsch, C.M., Cullen, J.J., Lapointe, B., Phinney, D.A., and Yentsch, S.W., 2002, Sunlight and water transparency: cornerstones in coral research: Journal of Experimental Marine Biology and Ecology, v. 268, p. 171-183.

FIGURE CAPTIONS

Figure 1A. Topography of Kaua‘i, derived from 10-meter DEM. Figure 1B. Geologic map of Kaua‘i, modified from Sherrod et al. (2007).

Figure 2A. Basin-averaged erosion rates on Kaua‘i, inferred from the volume of rock eroded from drainage basins since construction of each basin's initial topographic surface. The area of the circular symbol associated with each basin is proportional to the basin's erosion rate E_V. The black fraction of the circular symbol indicates the fraction f_V of the basin's initial rock volume that has been eroded. The number next to each circular symbol is the basin's ID in Table 1. The background color is the modern annual precipitation rate, resampled to 10 m resolution (Daly et al., 2002; PRISM Climate Group, Oregon State University). Figure 2B. Basin-averaged erosion rates vs. basin-averaged modern mean annual precipitation. Figure 2C. The extent of basin excavation vs. basin-averaged modern mean annual precipitation.

Figure 3. Hanalei River basin topography (background color) and detrital olivine sampling sites (black circles) for ^{3}He analysis. At right are sampling site names and minimum bounds on ^{3}He-inferred erosion rates calculated with Equation 2. Solid lines outline the Hanalei River basin and the subcatchments upstream of the sample sites. Dashed line separates the low-relief eastern Hanalei basin from the high-relief western Hanalei basin, to which separate spline surfaces were fit in the calculation of eroded volumes with Equation 1 (see Methods).

Figure 4A and 4B. Landslide scars in the Hanalei basin, in August 2006 (Figure 4A) and September 2003 (Figure 4B), each approximately 6-12 meters in width. Figure 4C. Hanalei River basin, looking south from a vantage point 1.95 km south-southwest of the USGS gauging station (Figure 3).

Figure 5. Upper panels: Satellite imagery used to map landslide scars in the Hanalei basin. Black line shows outline of the Hanalei basin. Lower panels: At left, the black line outlines the location of a landslide scar that is present in the WorldView-2 image but not in the Quickbird image. The upper right corner of the Quickbird image also shows a landslide scar that revegetated by the time the WorldView-2 image was taken nearly six years later.

Figure 6. Erosion rates in Kaua‘i’s Hanalei basin derived from four sets of measurements, each averaged over a different timescale. Open upper error bars on ^{3}He data points imply unbounded upper uncertainties on ^{3}He-based erosion rates.

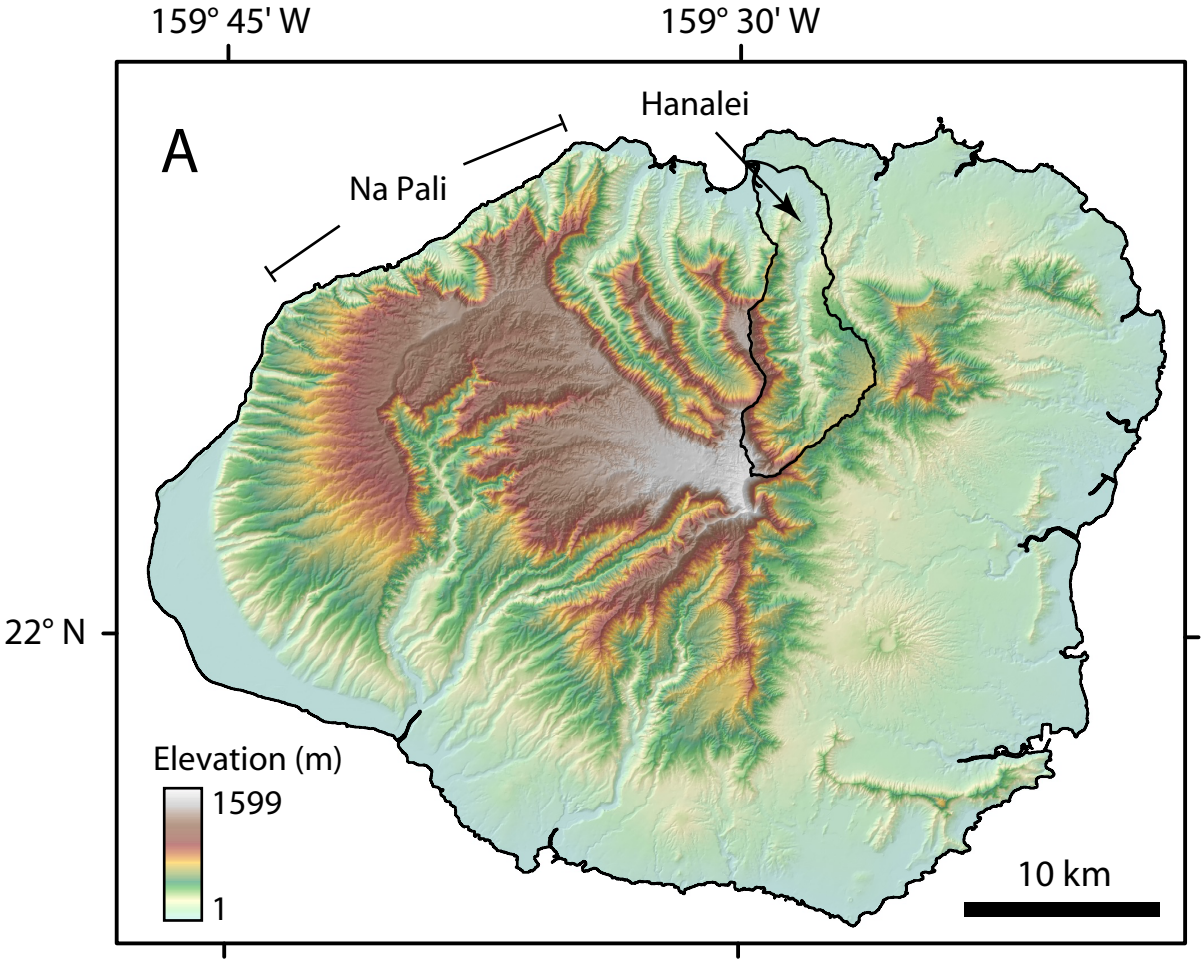
159° 45' W
159° 30' W
A
Hanalei
Na Pali
22° N
Elevation (m)
1599
1
10 km

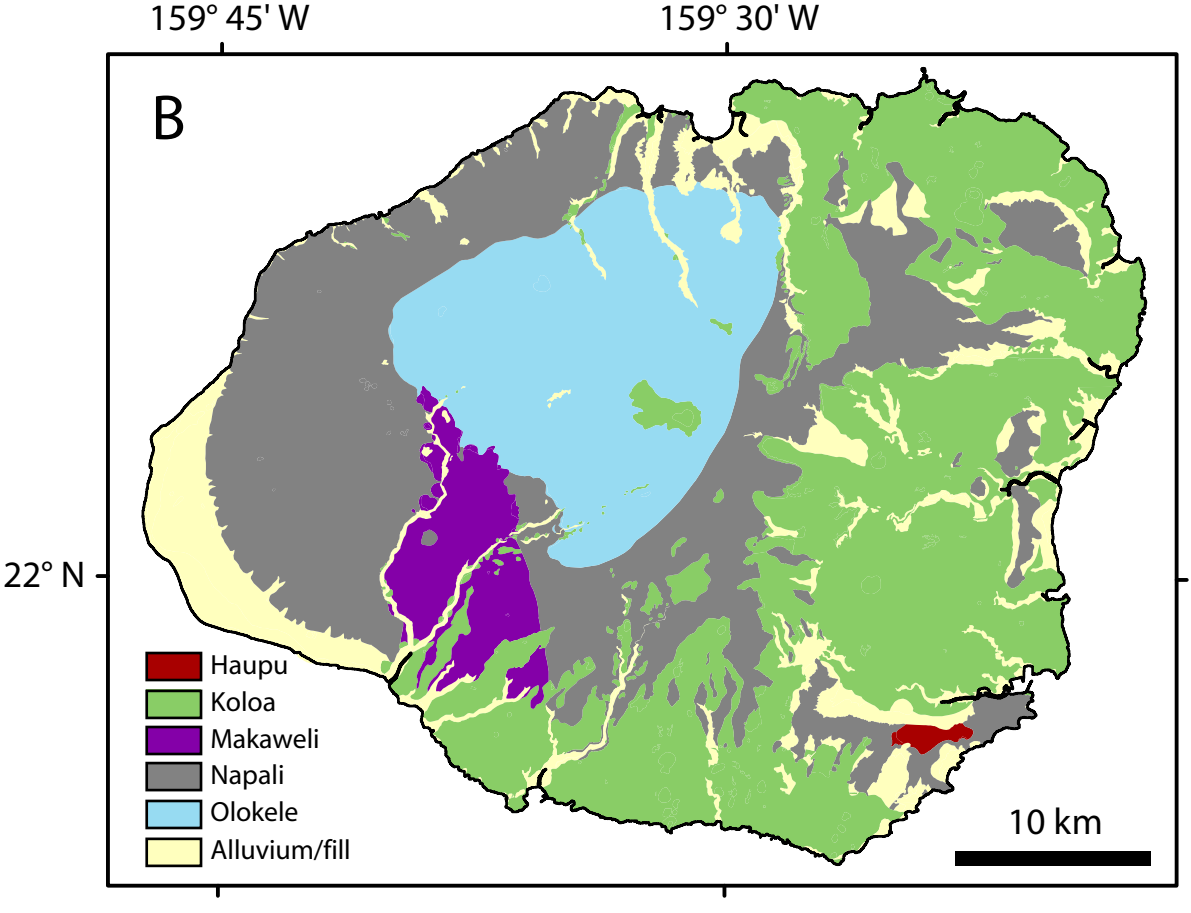
159° 45' W
159° 30' W
B
22° N
Haupu
Koloa
Makaweli
Napali
Olokele
Alluvium/fill
10 km

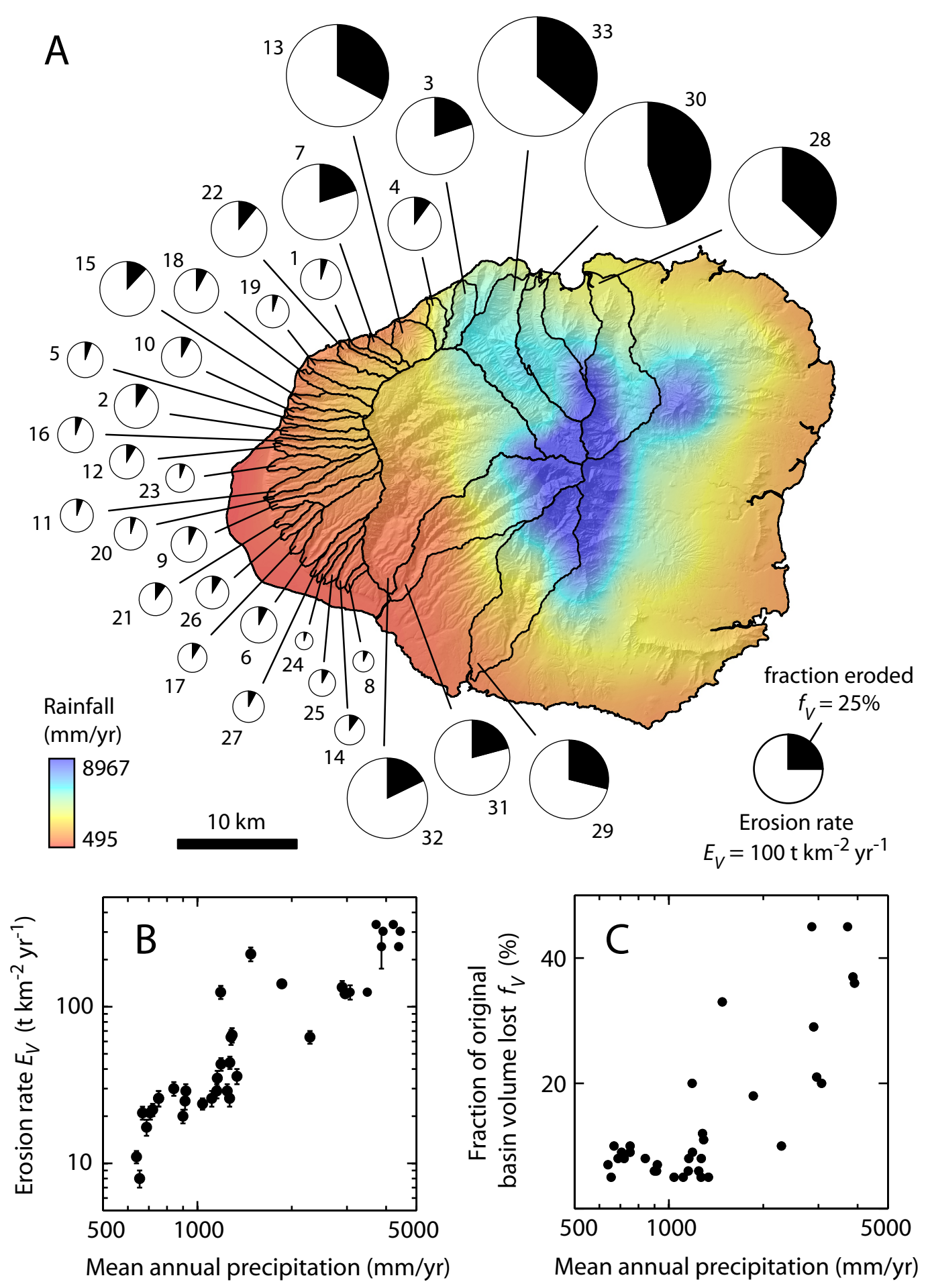
A
13
33
3
30
28
7
4
22
1
15
18
19
5
10
2
16
12
23
11
20
9
21
26
6
24
8
17
25
27
14
32
31
29
Rainfall
(mm/yr)
8967
495
10 km
fraction eroded
$f_V = 25\%$
Erosion rate
$E_V = 100$ t km^{-2} yr^{-1}
B
Erosion rate E_V (t km^{-2} yr^{-1})
100
10
500
1000
5000
Mean annual precipitation (mm/yr)
C
Fraction of original
basin volume lost f_V (%)
40
20
500
1000
5000
Mean annual precipitation (mm/yr)

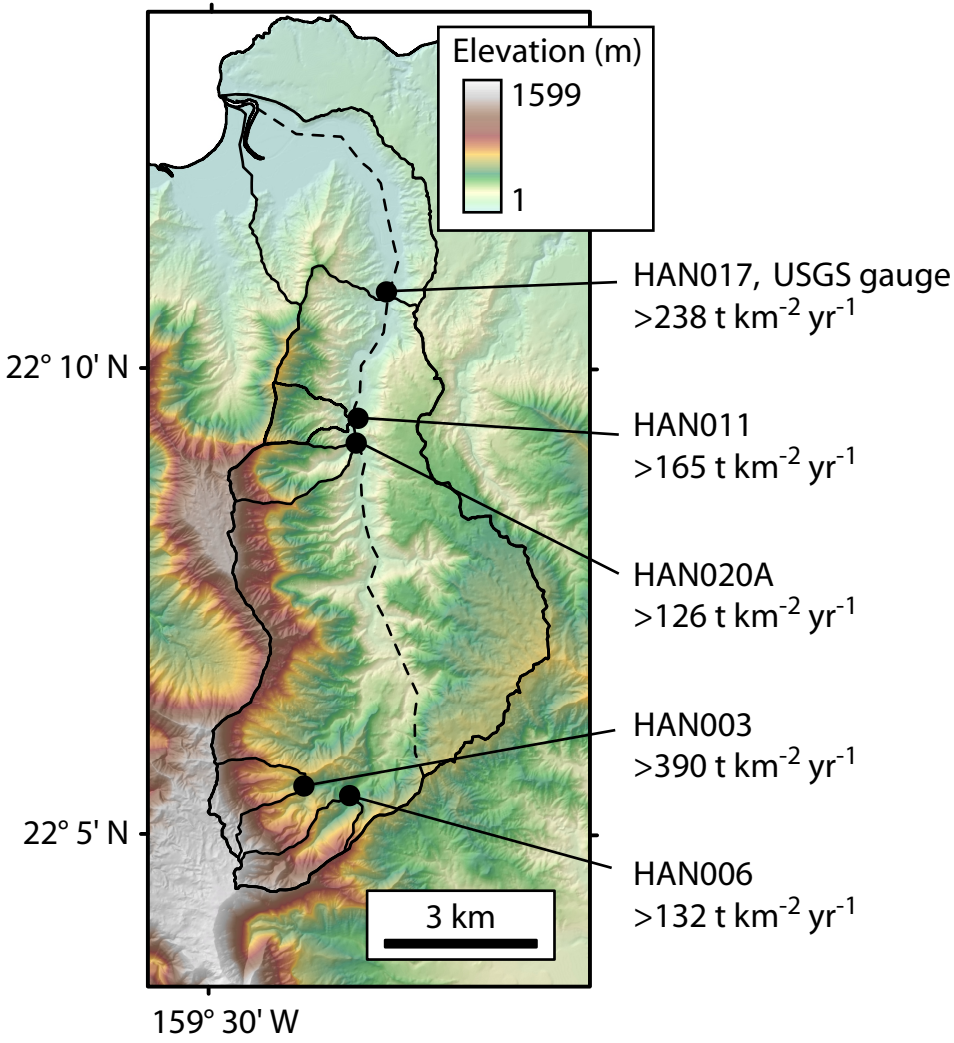
Elevation (m)
1599
1
HAN017, USGS gauge
>238 t km-2 yr-1
22° 10' N
HAN011
>165 t km-2 yr-1
HAN020A
>126 t km-2 yr-1
HAN003
>390 t km-2 yr-1
22° 5' N
HAN006
>132 t km-2 yr-1
3 km
159° 30' W

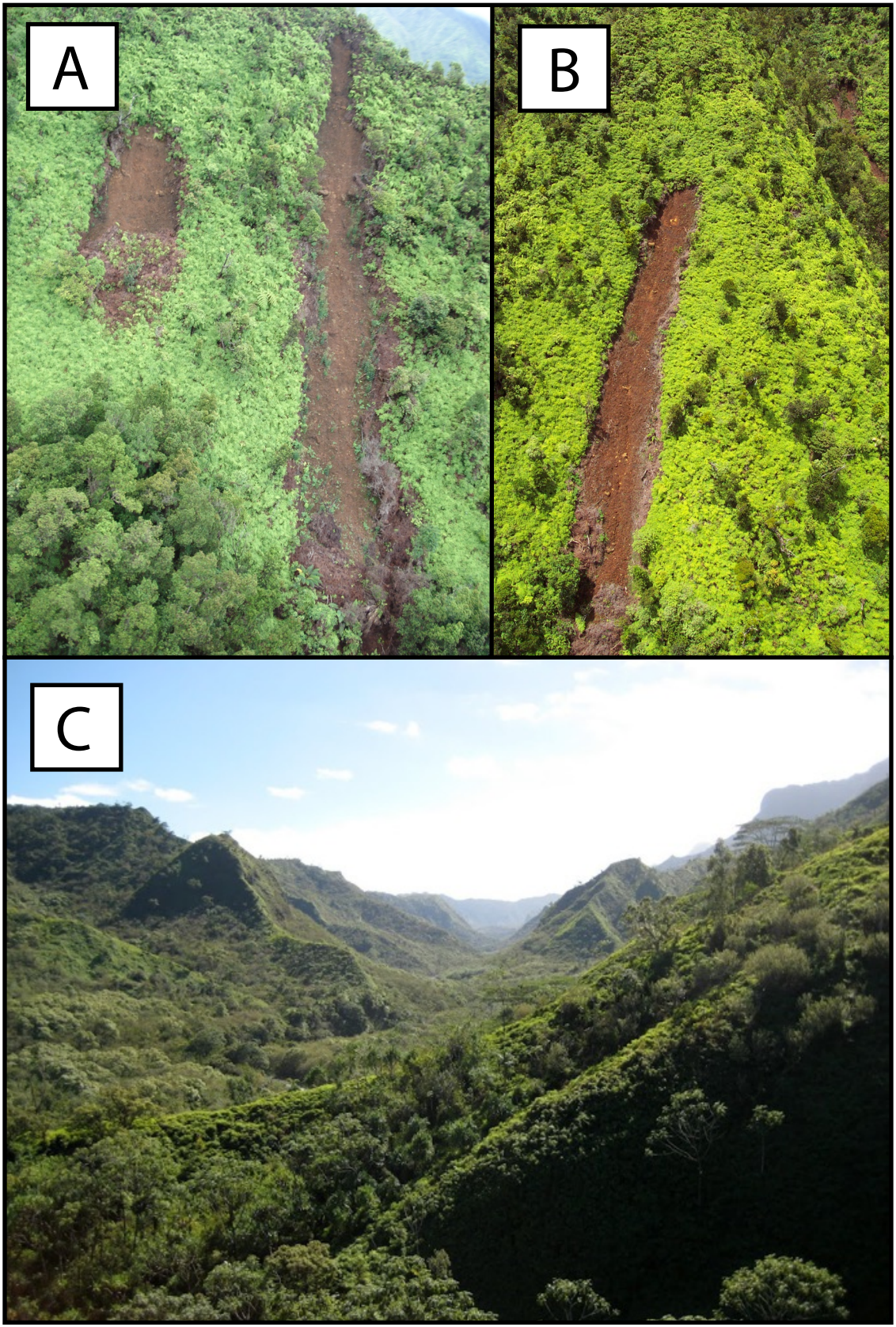
A
B
C

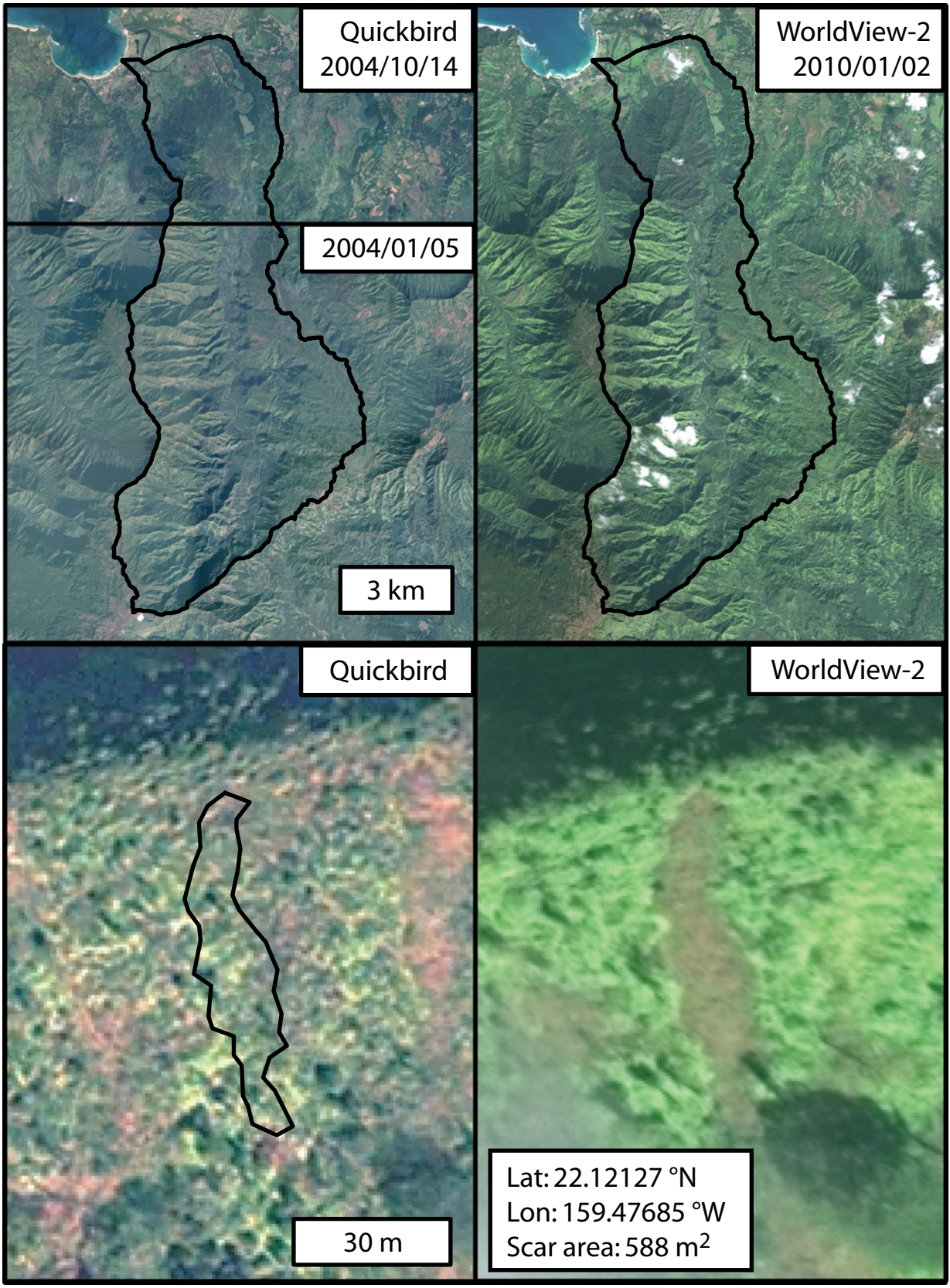
Quickbird
2004/10/14
2004/01/05
3 km
WorldView-2
2010/01/02
Quickbird
30 m
WorldView-2
Lat: 22.12127 °N
Lon: 159.47685 °W
Scar area: 588 m2

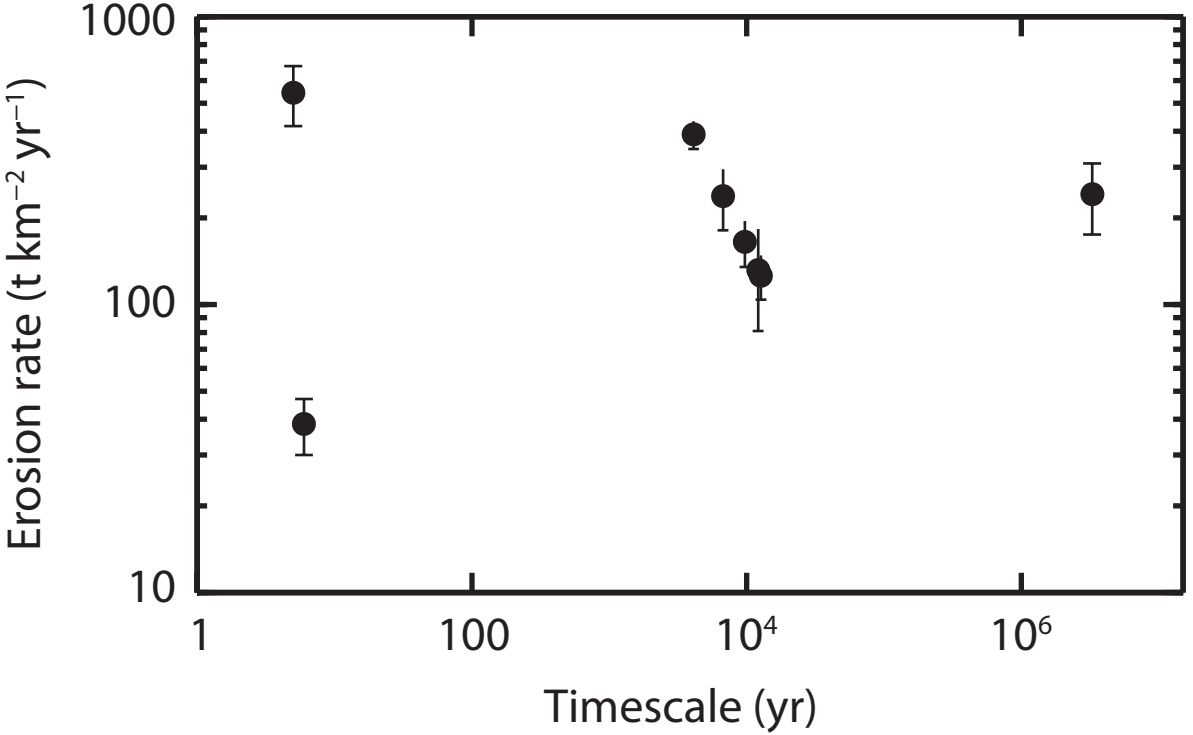
1000
100
10
Erosion rate (t km^{-2} yr^{-1})
1
100
10^4
10^6
Timescale (yr)